

Dynamical Response to the QBO in the Northern Winter Stratosphere: Signatures in Wave Forcing and Eddy Fluxes of Potential Vorticity

IAN P. WHITE

British Antarctic Survey, Cambridge, and Department of Electronic and Electrical Engineering, University of Bath, Bath, United Kingdom

HUA LU

British Antarctic Survey, Cambridge, United Kingdom

NICHOLAS J. MITCHELL

Department of Electronic and Electrical Engineering, University of Bath, Bath, United Kingdom

TONY PHILLIPS

British Antarctic Survey, Cambridge, United Kingdom

(Manuscript received 8 December 2014, in final form 19 May 2015)

ABSTRACT

Wave–mean flow interactions associated with the Holton–Tan effect (HTE), whereby the tropical quasi-biennial oscillation (QBO) modulates the Northern Hemisphere wintertime stratospheric polar vortex, are studied using the ERA-Interim dataset. Significant evidence of the HTE in isentropic coordinates is found, with a weaker and warmer polar vortex present when the lower-stratospheric QBO is in its easterly phase (QBOe). For the first time, the authors quantify the QBO modulation of wave propagation, wave–mean flow interaction, and wave decay/growth via a calculation of potential vorticity (PV)-based measures, the zonal-mean momentum budget, and up-/downgradient eddy PV fluxes. The effect of the tropospheric subtropical jet on QBO modulation of the wave activity is also investigated. In the subtropical-to-midlatitude lower stratosphere, QBOe is associated with an enhanced upward flux of wave activity, and corresponding wave convergence and wave growth, which leads to a stronger poleward zonal-mean meridional circulation and consequently a warmer polar region. In the middle stratosphere, QBOe is associated with increased poleward wave propagation, leading to enhanced wave convergence and in situ wave growth at high latitudes and contributing to the weaker polar vortex. In agreement with recent studies, the results suggest that the critical-line effect cannot fully account for these wave anomalies associated with the HTE. Instead, it is suggestive of a new, additional mechanism that hinges on the QBO-induced meridional circulation effect on the latitudinal positioning of the subtropical jet. Under QBOe, the QBO-induced meridional circulation causes a poleward shift of the subtropical jet, encouraging more waves to propagate into the stratosphere at midlatitudes.

1. Introduction

The most prominent feature of the winter stratosphere is the polar vortex: the cyclonic westerly winds that circumnavigate the pole, playing an important role in the dynamical circulation and the distribution of trace gases (e.g.,

Plumb 2002). The polar vortex can initiate tropospheric changes, including the transfer of tropical variations to midlatitudes, an altering of the storm tracks, and a modulation of near-surface weather patterns (e.g., Baldwin and Dunkerton 2001; Thompson et al. 2002; Bell et al. 2009), via a downward migration of zonal-mean zonal wind and temperature anomalies. Thus, understanding the physical mechanisms that cause variations of the polar vortex is vital to studying climate variability.

The quasi-biennial oscillation (QBO), an oscillation of easterly and westerly jets in the tropical stratosphere

Corresponding author address: Ian P. White, British Antarctic Survey, High Cross, Madingley Road, Cambridge CB3 0ET, United Kingdom.
E-mail: iwhit@bas.ac.uk

that descends from 3 to 70 hPa over a period of approximately 28 months, is one of the major factors that affect interannual variability of the polar vortex (Baldwin et al. 2001). One intriguing feature of the Northern Hemisphere (NH) winter is a phenomenon known as the Holton–Tan effect (HTE; Holton and Tan 1980), whereby a stronger polar vortex exists when the QBO is in the lower stratosphere (~ 50 hPa) is in its westerly phase (QBOw), and, conversely, a weaker polar vortex exists when the QBO is in its easterly phase (QBOe; Holton and Tan 1980). The HTE also holds when the QBO is defined by the vertical wind shear between 50 and 70 hPa, but it tends to be weaker for the QBO defined at other levels (Hitchman and Huesmann 2009, hereafter HH09). The HTE has been confirmed by observational studies (e.g., Dunkerton and Baldwin 1991; Naito and Hirota 1997; Lu et al. 2008, 2014) as well as by both mechanistic (e.g., O’Sullivan and Young 1992; Naito and Yoden 2006; Pascoe et al. 2006) and complex general circulation models (e.g., Calvo et al. 2009; Marshall and Scaife 2009). However, the mechanism behind the HTE is still under debate (e.g., Naoe and Shibata 2010; Yamashita et al. 2011; Garfinkel et al. 2012; Lu et al. 2014).

The polar vortex is most sensitive to planetary-scale Rossby waves propagating upward from the troposphere (e.g., McIntyre 1982). In extreme cases, these wave disturbances can cause rapid breakdowns of the vortex and rising temperatures in the polar stratosphere, a phenomenon known as a stratospheric sudden warming (SSW; Labitzke 1982). It has been found that SSWs tend to occur more frequently under QBOe than under QBOw conditions (e.g., Dunkerton and Baldwin 1991; Naito and Hirota 1997; Lu et al. 2008); thus, it is natural to suspect that a QBO modulation of planetary waves is responsible for the changes in the frequency of SSWs and the overall polar vortex strength (Holton and Tan 1980; Calvo et al. 2009).

A number of mechanisms have been proposed for the HTE, the most well-known of which was proposed by Holton and Tan (1980). It involves changes in the width of the extratropical waveguide and, consequently, the propagation of quasi-stationary planetary waves as a result of a latitudinal shift in the subtropical critical line (Holton and Tan 1980). Under QBOe conditions, the critical line in the lower stratosphere is located farther poleward in the NH, resulting in a narrower extratropical waveguide and, hence, a confinement of upward planetary wave fluxes from the troposphere to the stratosphere, to high latitudes. Furthermore, waves with small enough amplitude are reflected poleward by the critical line, causing a more disturbed polar vortex (Tung 1979). Conversely, under QBOw, the critical line

is located in the summer hemisphere, resulting in a latitudinally wider extratropical waveguide and allowing for more wave propagation away from the polar vortex. This leads to a less-disturbed, stronger, and colder vortex. This mechanism is referred to as the HT mechanism herein.

Efforts to verify the HT mechanism have not been very successful. For instance, Holton and Tan (1982) examined the Eliassen–Palm (EP) fluxes and EP flux divergence but could not establish statistically significant differences between different QBO phases. Dunkerton and Baldwin (1991) found that the QBO modulation of the EP flux was consistent with the observed wind anomaly but that there were only marginal differences in planetary wave amplitudes and the number of planetary wave events between the two QBO phases. Modeling studies have suggested that the QBO does cause changes in planetary wave amplitude in addition to changes in the EP flux and EP flux divergence (e.g., Holton and Austin 1991; Naito and Yoden 2006; Calvo et al. 2009; Watson and Gray 2014), although exactly how the QBO induces these wave changes remains unclear (Anstey and Shepherd 2014).

There have been a number of recent studies that have suggested that the changes in EP fluxes between QBOe and QBOw may be caused by something other than a change of waveguide in the lower stratosphere (e.g., Naoe and Shibata 2010; Yamashita et al. 2011; Garfinkel et al. 2012; Lu et al. 2014). For instance, Naoe and Shibata (2010) found quite the opposite to the HT mechanism; planetary waves tend to propagate more equatorward and upward in the midlatitude lower stratosphere under QBOe than under QBOw. By imposing easterly wind anomalies at different altitudes throughout the tropical stratosphere, Gray et al. (2001, 2004) found that the polar winds and temperatures are most sensitive to wind changes in the tropical and subtropical upper stratosphere, with easterly anomalies in the tropical upper stratosphere leading to an earlier onset of SSWs in comparison to their control simulations. These authors suggested that planetary waves of deep vertical structure are modulated by the subtropical upper-stratospheric wind anomalies associated with the QBO modulation of the critical line in the upper stratosphere.

Another mechanism, related to the QBO-induced secondary meridional circulation and the effect it has on wave propagation in the middle-to-upper stratosphere, has been suggested by Ruzmaikin et al. (2005) and recently supported by Garfinkel et al. (2012) and Lu et al. (2014). In this mechanism, an anomalously strong meridional circulation under QBOe creates a barrier for equatorward wave propagation in the middle-to-upper stratosphere, hence encouraging poleward planetary wave

propagation and resulting in enhanced EP flux convergence at high latitudes. Such modulation is not consistent with the HT mechanism, whereby, along with an overall poleward shift of upward-propagating wave activity, vertically alternating poleward, equatorward, and poleward wave propagation in the lower, middle, and upper stratosphere, respectively, is expected. However, a modeling study by Gray et al. (2003) found that a disturbed polar vortex can also be generated when a vertically deep easterly wind anomaly is imposed in the tropics. They consequently suggested that the QBO-induced meridional circulation, which is associated with a vertical wind shear in the tropics, is not required to produce the HTE and that instead the change in waveguide throughout the depth of the stratosphere associated with a critical-line shift is needed.

In studying the HTE, the most frequently used measures of wave activity are the EP fluxes and EP flux divergence, which give an indication of the net direction of wave propagation and wave drag imposed on the mean flow, and the refractive index, which identifies regions where wave propagation, wave absorption, and wave attenuation occur (e.g., Naoe and Shibata 2010; Garfinkel et al. 2012; Lu et al. 2014). An alternative way of measuring the wave–mean flow interaction involves potential vorticity (PV). In the absence of diabatic heating and friction, PV is conserved and advected along isentropic (i.e., potential temperature) surfaces so that there is no cross-isentropic movement of air (Haynes and McIntyre 1987). These properties make PV an ideal quantity to describe Rossby wave propagation in terms of meridionally displaced air parcels. Also, the meridional gradient of PV is an important parameter determining the refractive index (Matsuno 1970). Positive gradients, such as those associated with a positive wind shear, favor wave propagation, whereas negative gradients imply wave breaking (McIntyre and Palmer 1983).

PV-based metrics have been used to diagnose wave breaking both in the troposphere (e.g., Martius et al. 2007; Kunz et al. 2009) and the stratosphere (e.g., Baldwin and Holton 1988; Abatzoglou and Magnusdottir 2007; Hitchman and Huesmann 2007, HH09). For instance, Baldwin and Holton (1988) studied the climatology of planetary wave breaking at 850 K in the NH winter by defining wave breaking as a reversal in the meridional PV gradient. Studies have also utilized eddy fluxes of PV along isentropic surfaces to examine the diffusive properties of wave forcing (e.g., Butler et al. 2011; Birner et al. 2013). Birner et al. (2013) used the up-/down-PV-gradient eddy PV fluxes to investigate Rossby wave decay/growth in the vicinity of the tropospheric subtropical jet. However, there has been limited work that studies the HTE using PV on isentropic levels. One exception is HH09

who calculated a series of PV-based measures to determine the QBO modulation of Rossby wave propagation and breaking, finding a significant HTE during 1979–2002 in the reanalysis datasets they used.

The main objectives of this study are threefold: 1) to provide a comprehensive description of the climatology and QBO modulation of wave–mean flow interactions in the lower to middle stratosphere using an isentropic coordinate framework; 2) to extend the work of HH09 using a longer (1979–2012) and higher-resolution reanalysis dataset; and 3) to identify/corroborate a plausible mechanism that can explain why the HTE is strongly associated with the lower-stratospheric QBO in NH winter. To complete these objectives, we examine both the December–February (DJF)-mean climatology and composite differences of a series of PV-based measures developed by HH09, EP flux diagnostics, and eddy fluxes of PV. The majority of our analyses are based on the zonal-mean momentum budget and the wave-activity conservation law in the small-amplitude limit. For the third objective, we shall, in particular, explore the extent to which the QBO signatures of wave propagation, growth, and breaking support or conflict with the HT mechanism.

2. Theoretical framework

a. Potential vorticity in isentropic coordinates

The evolution of the PV field along potential temperature θ surfaces is often used to study large-scale Rossby wave propagation (Hoskins et al. 1985). In spherical isentropic coordinates, Rossby–Ertel's PV is defined by

$$P = \frac{1}{\sigma} \left[f - \frac{(u \cos \varphi)_\varphi}{a \cos \varphi} + \frac{v_\lambda}{a \cos \varphi} \right], \quad (1)$$

where u and v are the zonal and meridional velocities; λ and φ are the zonal and meridional coordinates; f , g , and a are the Coriolis parameter, gravitational constant, and Earth's radius; $\sigma = -g^{-1} \partial p / \partial \theta$ is the isentropic density; and p is the pressure. Subscripts denote partial derivatives with respect to the given variable.

In the NH winter stratosphere, the meridional PV gradient \bar{P}_φ is generally positive, which allows Rossby wave propagation (Charney and Drazin 1961). Negative \bar{P}_φ indicates wave breaking, whereby a wave's amplitude has grown to be sufficiently large so that the horizontal and/or vertical wind shear acts to topple the wave over, causing the undulating PV contours to overturn irreversibly (McIntyre and Palmer 1983). When wave breaking occurs on the edge of the polar vortex, where

\overline{P}_φ is strongly positive, filaments of high PV are stripped off and advected into lower latitudes, where they are subsequently mixed and homogenized in the surf zone.

b. Zonal-mean momentum equation

The zonal-mean momentum budget relates the mean-flow acceleration to the residual circulation and wave forcing. In spherical isentropic coordinates, it is expressed as (Andrews et al. 1987)

$$\begin{aligned} \frac{\partial \overline{u}}{\partial t} = & -\hat{v} \left[\frac{1}{a \cos \varphi} (\overline{u} \cos \varphi)_\varphi - f \right] - \hat{Q} \overline{u}_\theta \\ & + \frac{1}{\overline{\sigma} a \cos \varphi} \nabla \cdot \mathbf{F} - \frac{1}{\overline{\sigma}} (\overline{\sigma' u'})_t + D_1, \end{aligned} \quad (2)$$

where the overbar, prime, and hat respectively represent a zonal-mean, departure from the zonal-mean, and density-weighted zonal averages (e.g., $\hat{v} \equiv \overline{\sigma v / \sigma}$); Q is the diabatic heating rate; D_1 groups other nonconservative effects (both friction and other diabatic heating terms); and $\nabla \cdot \mathbf{F}$ is the EP flux divergence given by

$$\nabla \cdot \mathbf{F} = \frac{1}{a \cos \varphi} \frac{\partial}{\partial \varphi} (F^{(\varphi)} \cos \varphi) + \frac{\partial F^{(\theta)}}{\partial \theta}, \quad (3)$$

where $F^{(\varphi)} = -a \overline{\sigma' \overline{u' u'}} \cos \varphi$ and $F^{(\theta)} = g^{-1} \overline{p' \Psi'_\lambda}$ are the horizontal and vertical components of the EP flux vector $\mathbf{F} = (F^{(\varphi)}, F^{(\theta)})$, commonly used to represent the direction of wave propagation, where p is the pressure, and $\Psi \equiv c_p T + \Phi$ is the Montgomery streamfunction, with T the temperature, c_p the specific heat capacity at constant pressure, and Φ the geopotential. Note that the EP flux vector has been approximated using the small-amplitude assumption (i.e., $|B'| \ll |\overline{B}|$ for any field B) in order to be consistent with the wave-activity conservation law presented later in section 2c. The horizontal component $F^{(\varphi)}$ and the vertical component $F^{(\theta)}$ are the eddy momentum flux and the form drag, respectively [see Andrews (1983) for a discussion]. In Eq. (2), (\hat{v}, \hat{Q}) is the natural analog to the residual mean meridional circulation defined in log–pressure coordinates (Andrews 1983). Note that we have followed the convention in Andrews (1987) and included the perturbation diabatic heating term $[-(a \overline{\sigma' Q' u'} \cos \varphi)_\theta]$ in D_1 , as opposed to in $\nabla \cdot \mathbf{F}$. This better facilitates our study of the QBO modulation of the large-scale wave forcing.

Equation (2) states that the zonal-mean-flow tendency $\partial \overline{u} / \partial t$ evolves according to the horizontal wind shear and Coriolis acceleration acting on the residual mean meridional circulation $\{\Theta = -\hat{v}[(\overline{u} \cos \varphi)_\varphi / a \cos \varphi - f]\}$, upwelling and downwelling induced by the vertical wind shear $(-\hat{Q} \overline{u}_\theta)$, the EP flux divergence term ($\Pi = \nabla \cdot \mathbf{F} / \overline{\sigma} a \cos \varphi$) representing the resolved-wave forcing,

effects related to small-scale gravity waves $[(\overline{\sigma' u'})_t / \overline{\sigma}]$; e.g., Edouard et al. 1997], and other eddy and mean-flow nonconservative processes D_1 . In the seasonal mean, Π tends to approximately balance Θ (i.e., $\Theta + \Pi \approx 0$) so that a negative Π anomaly signifies a strengthened poleward residual mean meridional circulation Θ and weaker polar vortex, and vice versa (Newman et al. 2001; Lu et al. 2014).

The EP flux divergence term Π in Eq. (2) can be linked to eddy PV fluxes by

$$\overline{\sigma' v' P'} = \Pi - \frac{(\overline{\sigma' u'})_t}{\overline{\sigma}} + D_2 + O(3), \quad (4)$$

where D_2 represents nonconservative terms, and $O(3)$ are nonlinear terms of order 3 or higher in perturbation variables (Andrews 1987). The meridional eddy PV fluxes $\overline{\sigma' v' P'}$ represent a meridional redistribution of PV, with $\overline{\sigma' v' P'} < 0$ indicating equatorward fluxes and $\overline{\sigma' v' P'} > 0$ indicating poleward fluxes. According to Eq. (4), $\overline{\sigma' v' P'}$ is contributed to by the resolved-wave forcing Π , small-scale gravity wave effects $-(\overline{\sigma' u'})_t / \overline{\sigma}$, nonconservative effects D_2 , and additional nonlinear effects. Upon substitution into Eq. (2), $\overline{\sigma' v' P'}$ must nearly balance Θ in the seasonal mean so that equatorward fluxes ($\overline{\sigma' v' P'} < 0$) tend to strengthen the poleward residual mean meridional circulation (i.e., $\Theta > 0$), and vice versa. Because the main focus of this study is on the QBO modulation of large-scale wave forcing and circulation in the lower to middle stratosphere, where the effect of small-scale wave forcing is small, we group the contribution of the latter three terms in Eq. (4) into a single term, denoted D herein.

c. Wave-activity conservation law

Starting from the linearized PV wave equation for P' (i.e., under the small-amplitude assumption), the wave-activity conservation law is expressed as (Andrews 1987)

$$\frac{\partial \overline{P'^2}}{\partial t} = -\frac{2 \overline{v' P' P'_\varphi}}{a} + D_3 + O(3), \quad (5)$$

where $\overline{P'^2}$ is here defined as a measure of the wave activity. Equation (5) states that the wave-activity decay/growth in time $\partial \overline{P'^2} / \partial t$ is affected by up-/downgradient eddy PV fluxes $2 \overline{v' P' P'_\varphi} / a$, nonconservative processes D_3 , and nonlinear terms $O(3)$, where the terms on the right-hand side act as either a source or a sink of wave activity. More specifically, downgradient eddy PV fluxes ($2 \overline{v' P' P'_\varphi} / a < 0$) correspond to wave-activity growth ($\partial \overline{P'^2} / \partial t > 0$), whereas upgradient eddy PV fluxes ($2 \overline{v' P' P'_\varphi} / a > 0$) correspond to wave-activity decay ($\partial \overline{P'^2} / \partial t < 0$). In the NH winter

stratosphere, where \bar{P}_ϕ is generally positive, we expect that downgradient eddy PV fluxes (i.e., wave growth) dominate Eq. (5), corresponding to equatorward eddy PV fluxes ($\overline{v'P'} < 0$) and a reduced angular momentum of the mean flow. Conversely, upgradient eddy PV fluxes are less expected, instead leading to a local, enhanced angular momentum of the mean flow (e.g., Vallis 2006). We define $\Gamma = 2\overline{v'P'P_\phi}/a$ for simplicity.

The approximate decay/growth of the resolved waves can be further estimated by substituting Eq. (4) into Eq. (5) to find

$$\frac{\partial \overline{P'^2}}{\partial t} = -\frac{2\mathbf{V} \cdot \mathbf{F}}{a^2 \bar{\sigma}^2 \cos \phi} \bar{P}_\phi + \frac{2(\overline{\sigma' u'})_t}{a \bar{\sigma}^2} \bar{P}_\phi + D_4 + O(3), \quad (6)$$

where D_4 represents nonconservative terms combined from D_2 and D_3 . We define $\Gamma_{\text{Res}} = 2\bar{P}_\phi \mathbf{V} \cdot \mathbf{F}/a^2 \bar{\sigma}^2 \cos \phi$ for notational simplicity. In a region where \bar{P}_ϕ is positive and the EP flux divergence is negative ($\mathbf{V} \cdot \mathbf{F} < 0$), waves would be expected to propagate into that region. We would therefore also expect to find $\Gamma_{\text{Res}} < 0$ and, consequently, a growth in wave activity ($\partial \overline{P'^2}/\partial t > 0$). Conversely, if \bar{P}_ϕ is positive but the EP flux divergence is also positive ($\mathbf{V} \cdot \mathbf{F} > 0$), it is expected that waves would propagate away from that region. This should be accompanied by $\Gamma_{\text{Res}} > 0$ and, thus, a decay in wave activity ($\partial \overline{P'^2}/\partial t < 0$). When a theoretical equation such as Eq. (6) is evaluated using reanalysis datasets, where the perturbation is limited by the model resolution, Γ_{Res} refers to resolved-wave transience; it is distinct from Γ , which includes the contribution from resolved waves and subgrid processes, such as the gravity wave term and nonconservative effects.

The zonal-mean momentum budget expressed by Eqs. (2)–(4) allows us to examine the effect of waves on the zonal-mean circulation by evaluating the wave forcing in terms of the EP flux divergence term Π or the meridional eddy flux of PV $\overline{\sigma v'P'}$. Equations (5) and (6) provide us a means to study the wave decay/growth. These equations are intrinsically linked by Π or $\overline{\sigma v'P'}$. Together, they give a comprehensive description of the temporal change of both the waves and the mean flow.

3. Data and methods

Here, we use daily averages estimated from 6-hourly ERA-Interim data, with a horizontal resolution of 0.7° from the European Centre for Medium-Range Weather Forecasts (ECMWF; Dee et al. 2011; see www.ecmwf.int) for the period of 1979–2012. From this dataset, we use PV data on nine isentropic levels from 350 to 850 K (~ 150 – 10 hPa or 10 – 33 km). Additionally, we use the horizontal wind field u and v , temperature T , and geopotential height

Z , which have been interpolated from the archived 37 pressure levels to the same nine isentropic levels as the PV data using a piecewise cubic Hermite interpolating polynomial. Of the 37 pressure levels, approximately 10 are spanned by the 350- and 850-K isentropic levels. We focus on the NH middle winter (DJF), during which the HTE bears its strongest signal and the stratospheric polar vortex is most variable (Dunkerton and Baldwin 1991). For brevity, the year associated with each DJF period is defined by the year in which December falls (e.g., the year labeled as 1986 indicates the winter period from December 1986 to February 1987).

Three PV-based measures developed by HH09 are adopted here to examine wave propagation, wave breaking, and wave activity. They are as follows: (i) the zonal-mean meridional PV gradient \bar{P}_ϕ [units: $\text{K m}^2 \text{kg}^{-1} \text{s}^{-1} (1^\circ)^{-1}$]; (ii) the zonal-mean negative meridional PV gradient occurrence frequency $\bar{\gamma}$ (in days during DJF); and (iii) the zonal mean of the standard deviation of daily PV gradient values at each gridpoint $\bar{\xi}$ [units: $\text{K m}^2 \text{kg}^{-1} \text{s}^{-1} (1^\circ)^{-1}$]. The daily meridional PV gradient is calculated using forward differences from north to south of the daily mean PV at each grid point. The negative meridional PV gradient occurrence frequency is calculated by counting the total number of days in which a negative P_ϕ is found during DJF at each grid point. The daily variability of the meridional PV gradient ξ is calculated as the temporal variance of daily P_ϕ over DJF at each grid point. Each of P_ϕ , γ , and ξ are then zonally averaged to obtain \bar{P}_ϕ , $\bar{\gamma}$, and $\bar{\xi}$. We note here that the sign of \bar{P}_ϕ provides the key information on whether quasi-stationary planetary waves can propagate through a region, with a positive gradient indicating wave propagation can occur. A negative PV gradient, on the other hand, indicates either wave breaking, wave reflection, or wave instability via satisfaction of the Rayleigh–Kuo criterion, whereby new waves can be generated (e.g., Vallis 2006). Even so, in the NH winter stratosphere, planetary wave breaking is the dominant process associated with a negative PV gradient (e.g., McIntyre 1982). The variables $\bar{\gamma}$ and $\bar{\xi}$ are empirical measures of wave breaking and wave activity (HH09). To differentiate $\bar{\xi}$ from the wave activity $\overline{P'^2}$ defined in Eq. (5), we refer to $\bar{\xi}$ as the wave-activity proxy and $\overline{P'^2}$ as the wave activity.

Terms present in the zonal-mean momentum budget [Eqs. (2)–(4)] and the wave-activity conservation law [Eqs. (5) and (6)] are estimated based on daily PV and interpolated daily data of u , v , T , and Z in isentropic coordinates. See sections 2b and 2c for more details.

To define the QBO phase for each DJF period, we utilize the definition given in Huesmann and Hitchman (2001), which is also used by HH09, and calculate the vertical difference between the 50- and 70-hPa pressure

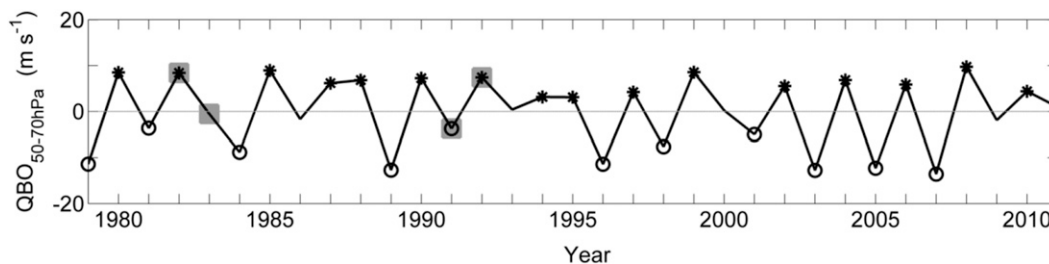


FIG. 1. Time series of DJF anomalies of the zonal-mean wind difference between the 50- and 70-hPa pressure surfaces, $QBO_{50-70hPa}$, averaged between $5^{\circ}S$ and $5^{\circ}N$. Note that the year labeled 1986 indicates the winter period from December 1986 to February 1987). Black star markers denote QBOw years, and black circle markers denote QBOe years. Gray square markers denote those years affected by two major volcanic eruptions. In total, excluding those four years affected by volcanoes, there are 14 QBOw and 10 QBOe winters.

surfaces (approximately 530- and 475-K isentropic surfaces, respectively) of the DJF-averaged zonal-wind anomalies averaged between $5^{\circ}S$ and $5^{\circ}N$. The sign and magnitude of this difference then determines the phase of the QBO, with a positive difference ($\geq 2 \text{ m s}^{-1}$) indicating QBOw and a negative difference ($\leq -2 \text{ m s}^{-1}$) indicating QBOe. All other DJF winters that do not satisfy either criterion are classified as neutral. We note that Huesmann and Hitchman (2001) used a different threshold of 1.5 m s^{-1} , although we find that this does not change any of our conclusions qualitatively. Here, we refer to our QBO definition as $QBO_{50-70hPa}$ or QBO for simplicity. The result of our definition for each DJF winter from 1979 to 2011 is shown in Fig. 1, with 16 QBOw, 11 QBOe, and 6 neutral winters overall. Composite differences between QBOe and QBOw ($QBOe - QBOw$) are calculated for all of the aforementioned quantities. The confidence levels for these differences are determined at the 90% and 95% levels using two-sided Student's t tests. For certain statistically significant regions (to be defined in the relevant sections), linear correlations between the relevant quantity and the QBO are performed, with the results shown as time series plots, to provide an appreciation of the temporal effect of the QBO. Also, we note that qualitatively similar results can be obtained if the QBO is defined as the wind anomalies at 50 hPa, because the QBO wind anomalies at 50 hPa are approximately twice as large as those at 70 hPa, and these two levels are usually in phase with one another (not shown).

To account for the possible contamination of the QBO signal by the two major volcanic eruptions (El Chichón, March 1982, and Mount Pinatubo, June 1991), which released large quantities of volcanic aerosols into the stratosphere and caused anomalous warming of the stratosphere for two years after the eruption, we exclude the four winters that fell into the periods of March 1982–February 1984 and June 1991–May 1993 (shown in Fig. 1 as gray square markers) from our composite analysis. This results in 14 QBOw and 10 QBOe winters overall. Sensitivity tests

nevertheless suggest that similar results can be obtained if those four winters are included in our composite analysis.

4. Results

a. The Holton–Tan effect in wind and temperature

In this section, the zonal-mean zonal wind \bar{u} and zonal-mean temperature \bar{T} are analyzed to quantify the QBO modulation of the stratospheric circulation during NH winter. This allows us to appreciate the extent to which the HTE holds when these primary variables are mapped to isentropic coordinates.

The DJF-mean climatology of \bar{u} is shown in Fig. 2a. The stratospheric winds are marked by westerlies that peak in the NH at around $60^{\circ}N$, forming the polar vortex at 500 K and above, and the easterly winds in the subtropical Southern Hemisphere (SH). The winter westerlies and summer easterlies are separated by the zero-wind line located in the tropical NH stratosphere. The tropospheric subtropical jet can also be seen at $30^{\circ}N$, 350–400 K. Figure 2b shows the QBO composite difference of \bar{u} . The vertically alternating negative and positive \bar{u} anomalies in the tropical stratosphere correspond to the QBO defined in Fig. 1. The HTE is also visible, with the polar vortex significantly weaker (by $\sim 10 \text{ m s}^{-1}$) under QBOe in comparison to QBOw. Downward-arching negative \bar{u} anomalies exist in the tropics to subtropics from the 450- to 350-K θ levels. They are accompanied by downward-arching positive \bar{u} anomalies in the subtropics to midlatitudes from the 850- to 350-K θ levels. The subtropical-to-midlatitude positive anomalies below 700 K constitute a region of enhanced baroclinicity and are likely caused by a downward descent of the subtropical \bar{u} anomalies from the middle stratosphere over winter (not shown). In the upper troposphere ($\sim 350 \text{ K}$), the combination of the negative \bar{u} anomalies at 20° – $30^{\circ}N$ and positive \bar{u} anomalies at 40° – $45^{\circ}N$ indicate a poleward shift of the subtropical jet under QBOe.

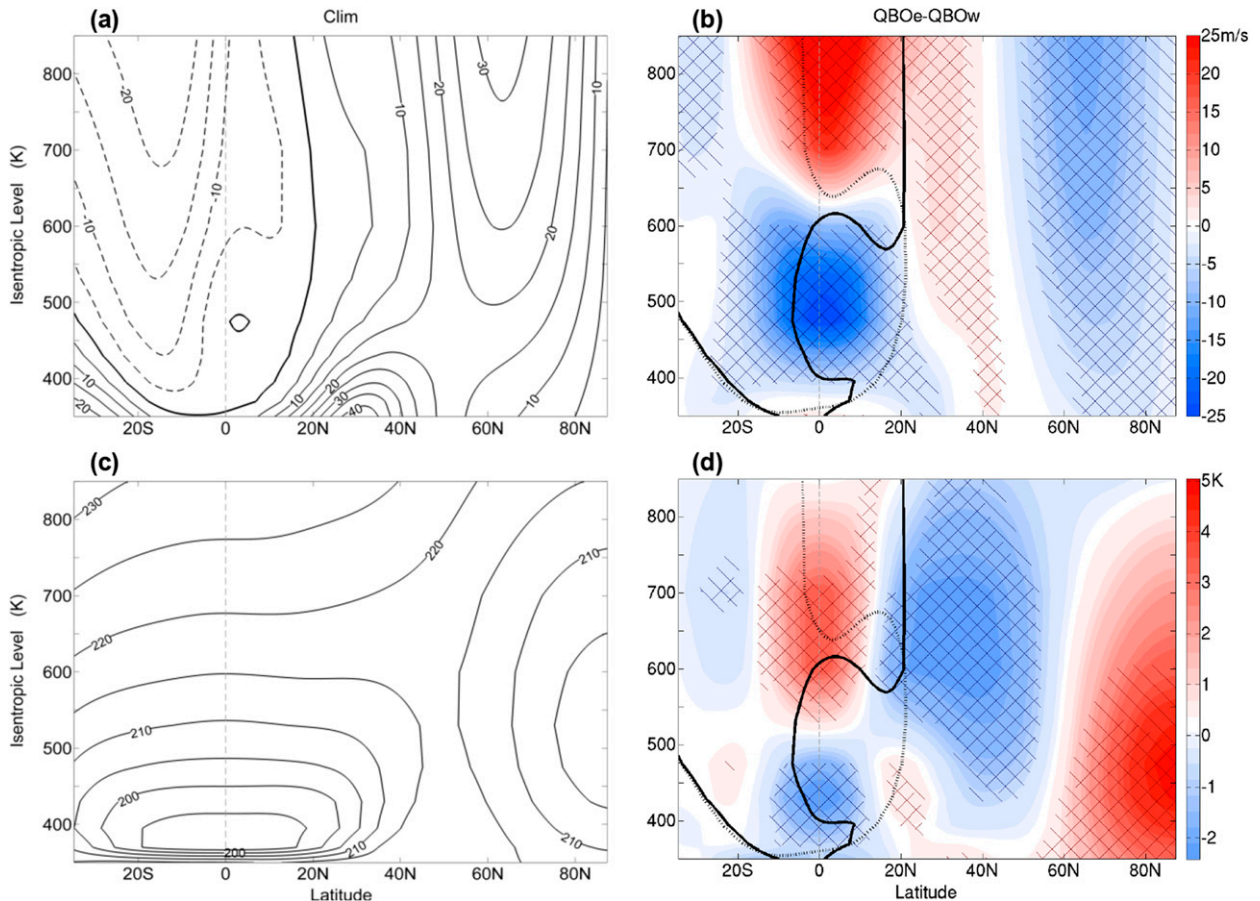


FIG. 2. (a) Climatology and (b) QBO composite difference (QBOe – QBOw) of the DJF-averaged zonal-mean zonal wind \bar{u} in the latitude–height plane. Contours (interval: 5 m s^{-1}) represent positive (solid) and negative (dashed) winds. The thick black line in (a) is the zero-wind line. In (b), the shading represents positive (i.e., westerly; red) and negative (i.e., easterly; blue) anomalies, the thick lines represent the zero-wind lines for QBOw (solid) and QBOe (dotted), and the hatching indicates statistical significance at the 90% (backward hatching) and 95% (forward hatching) levels. The dashed gray line represents the location of the equator. (c),(d) As in (a) and (b), but for the zonal-mean temperature \bar{T} and with a contour interval of 5 K in (c).

Figure 2c shows that the DJF-mean \bar{T} is marked by two cold regions: one just above the tropical tropopause, where the temperature falls to 195 K, and another one in the high-latitude lower stratosphere, where the temperature falls to 205 K. In the tropics, the QBO signature in \bar{T} is marked by a vertical dipole structure, with cold anomalies in the lower stratosphere and warm anomalies at the 550–700-K θ levels (Fig. 2d). They signify anomalous upwelling and downwelling due to the QBO-induced secondary meridional circulation, corresponding to the easterly and westerly tropical zonal-wind anomalies shown in Fig. 2b (Plumb and Bell 1982). At high latitudes, the QBO signature in \bar{T} is marked by warm anomalies in the lower stratosphere (60° – 90° N, 350–600 K), with a peak value of 5 K centered at the 450-K θ level near the pole. Cold anomalies are also present in the subtropics in the region of 600–800 K in both hemispheres. The effect is noticeably stronger in

the NH, with cold anomalies extending to midlatitudes and downward into the lower stratosphere. This seasonal asymmetry in the subtropical response to the QBO is known to be linked to the QBO-induced meridional circulation (Jones et al. 1998; Kinnersley 1999). These extratropical temperature anomalies are consistent with the wind anomalies shown in Fig. 2b and indicate an anomalous poleward meridional circulation that causes adiabatic heating at high latitudes under QBOe.

Figures 3a and 3b examine the temporal evolution of the high-latitude winds and temperature in relation to the QBO. It shows that the zonal-mean zonal wind anomalies, area weighted and averaged over 55° – 75° N, 700–850 K, correlates positively with the QBO ($r = 0.44$, $p = 0.01$), while the zonal-mean temperature anomaly, area weighted and averaged over 65° – 85° N, 430–600 K, is negatively correlated with the QBO ($r = -0.37$, $p = 0.035$). Together, they indicate that a significantly weaker,

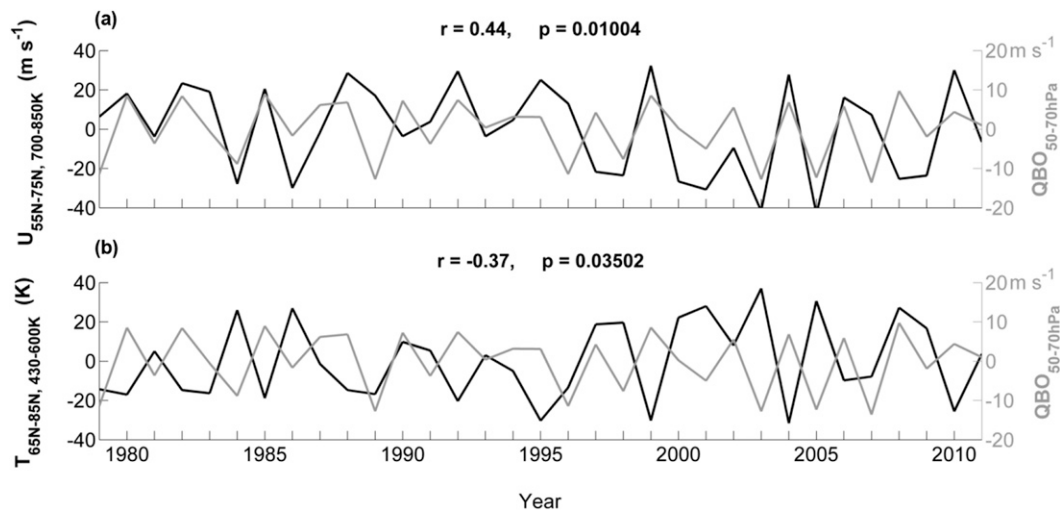


FIG. 3. (a) Time series of the DJF mean of \bar{u} , area weighted over 55° – 75° N and 700–850 K (black line), against the DJF-mean QBO wind shear as shown in Fig. 1 (gray line). The correlation coefficient r and p values are given just above the plot. (b) As in (a), but for the zonal-mean temperature averaged over 65° – 85° N and 430–600 K.

warmer polar vortex is associated with QBOe, agreeing with Figs. 2b and 2d and with previous studies based on pressure coordinates (e.g., Lu et al. 2014).

b. Effect on PV-based measures

In this section, we analyze a series of PV-based measures developed by HH09 (see section 3 for definition) in order to examine the climatology and the QBO modulation of wave activity and its preference to either propagate or break.

The zonal-mean meridional PV gradient \bar{P}_{ϕ} has been used previously by other studies to determine the ability of Rossby waves to propagate, with a positive \bar{P}_{ϕ} encouraging wave propagation. The climatology of \bar{P}_{ϕ} is shown in Fig. 4a. A peak in \bar{P}_{ϕ} occurs in the tropical lower stratosphere, flanked by relatively weak \bar{P}_{ϕ} ; this feature may be due to a combined inertial–barotropic instability, which during NH winter is associated with the cross-equatorial flow from the SH to the NH (e.g., Hitchman and Huesmann 2007). Another peak in \bar{P}_{ϕ} is also visible at 60° N and above the 600-K θ level, which corresponds to the edge of the polar vortex (Fig. 2a). A localized peak in \bar{P}_{ϕ} is also found at around 30° N, 350–400 K, corresponding to the tropospheric subtropical jet. These latter two peaks, coincident with the peak westerly winds, agree with the notion that regions with strong westerly winds act as waveguides, favoring wave propagation (Hoskins et al. 1985).

The QBO composite difference of \bar{P}_{ϕ} is shown in Fig. 4b. According to the climatological behavior of \bar{P}_{ϕ} , we expect more Rossby waves to propagate into the regions with enhanced \bar{P}_{ϕ} (i.e., red regions) and fewer

into regions with reduced \bar{P}_{ϕ} (i.e., blue regions). In the tropics, the QBO signature appears as vertically alternating negative and positive PV gradient anomalies, sharing the same sign as the QBO in zonal wind. Negative \bar{P}_{ϕ} anomalies are found at 60° – 80° N, extending from the lower stratosphere to the 850-K θ level, indicative of a weaker polar vortex under QBOe, in agreement with the HTE. Positive \bar{P}_{ϕ} anomalies are found in the subtropical-to-midlatitude lower stratosphere (10° – 30° N, 400–600 K) in both hemispheres, suggesting the ability for enhanced wave propagation in these regions under QBOe. The positive \bar{P}_{ϕ} anomalies in the NH, however, extend farther poleward to 45° N, while the SH counterpart is confined more equatorward at 10° – 30° S. Similar features exist at 10° – 20° N and above 600 K but with the opposite sign, indicating significant decreases in \bar{P}_{ϕ} in these regions. These subtropical \bar{P}_{ϕ} anomalies (up to 30° N) are mainly associated with the meridional wind shear associated with the QBO, whereas the extension of positive anomalies to mid-latitudes is associated with the downward-arching zonal winds in this region (Fig. 2b).

Negative PV gradients are associated with wave breaking. Hence, the occurrence frequency of zonal-mean negative gradients $\bar{\gamma}$ provides the information as to the regions where waves are most likely to break. The climatology of DJF-mean $\bar{\gamma}$ is shown in Fig. 4c. In general, regions where $\bar{\gamma}$ decreases tend to coincide with the regions where \bar{P}_{ϕ} increases. This is consistent with the notion that strong meridional PV gradients inhibit wave breaking. It is worth noting that, in the climatology, maximum $\bar{\gamma}$ values are found in the subtropics to

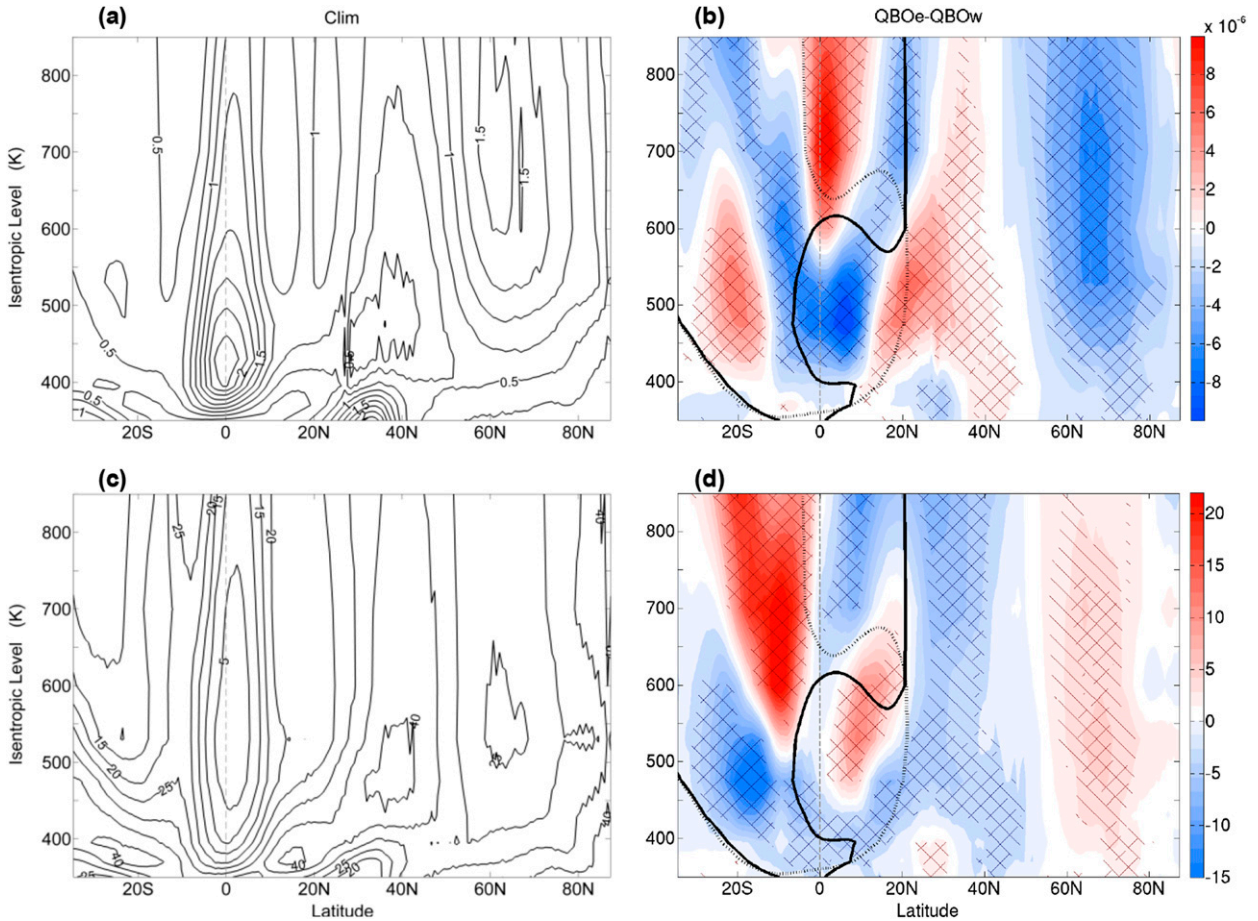


FIG. 4. (a),(b) As in Figs. 2a and 2b, but for the zonal-mean meridional PV gradient \bar{P}_ϕ [$\text{K m}^2 \text{kg}^{-1} \text{s}^{-1} (1^\circ)^{-1}$]. The climatology has a contour interval of $0.25 \times 10^{-5} \text{K m}^2 \text{kg}^{-1} \text{s}^{-1} (1^\circ)^{-1}$. Note that both climatology and composite difference have been scaled using the PV scaling developed by Lait (1994); for each isentropic level θ , we multiply \bar{P}_ϕ by $(\theta/350)^{-9/2}$ in order to account for the exponential decrease with height of PV in the plot. (c),(d) As in (a) and (b), but for the occurrence frequency of negative PV gradients $\bar{\gamma}$ (in days out of the total number of days in the DJF period), with a contour interval of 5 days in (c).

midlatitudes ($30^\circ\text{--}45^\circ\text{N}$) where PV gradient reversals occurred for 35–50 days during each DJF period on average. This is consistent with planetary wave breaking in the surf zone, stripping high PV filaments from the polar vortex edge and advecting them into lower latitudes (McIntyre and Palmer 1983).

Figure 4d shows the QBO composite difference of the DJF occurrence of $\bar{\gamma}$. Similar to its climatological behavior, regions with positive $\bar{\gamma}$ anomalies tend to coincide with regions of negative \bar{P}_ϕ anomalies. Positive $\bar{\gamma}$ anomalies are found in the tropical-to-subtropical NH lower stratosphere ($0^\circ\text{--}20^\circ\text{N}$, 475–600 K) and also in the tropical-to-subtropical SH middle stratosphere ($0^\circ\text{--}20^\circ\text{S}$, 600–850 K), consistent with wave breaking near the QBO critical line under QBOe. The large negative $\bar{\gamma}$ anomaly at $10^\circ\text{--}30^\circ\text{S}$, 430–530 K is also consistent with enhanced wave breaking near the QBO critical line under QBOw. At high latitudes, positive $\bar{\gamma}$ anomalies

appear inside the polar vortex, indicating increased wave breaking and corresponding dynamically to the negative \bar{u} anomalies at high latitudes under QBOe (Fig. 2b). The positive $\bar{\gamma}$ anomalies on the equatorward flank of the subtropical jet and negative $\bar{\gamma}$ anomalies on its poleward flank, correspond to a poleward shift of the jet under QBOe (Garfinkel and Hartmann 2011; also shown in Fig. 2b). At $25^\circ\text{--}40^\circ\text{N}$, 400–850 K, the negative $\bar{\gamma}$ anomalies are dynamically consistent with the stronger westerly winds in this region inhibiting wave breaking. The anomalous patterns of \bar{P}_ϕ and $\bar{\gamma}$ shown in Figs. 4b and 4d suggest that the QBO significantly modulates extratropical waveguides by allowing more planetary waves to propagate through midlatitudes ($\sim 35^\circ\text{--}50^\circ\text{N}$) and fewer planetary waves to propagate through high latitudes ($\sim 55^\circ\text{--}80^\circ\text{N}$) under QBOe.

The standard deviation of the daily meridional PV gradient $\bar{\xi}$ has been used by HH09 as a proxy for wave

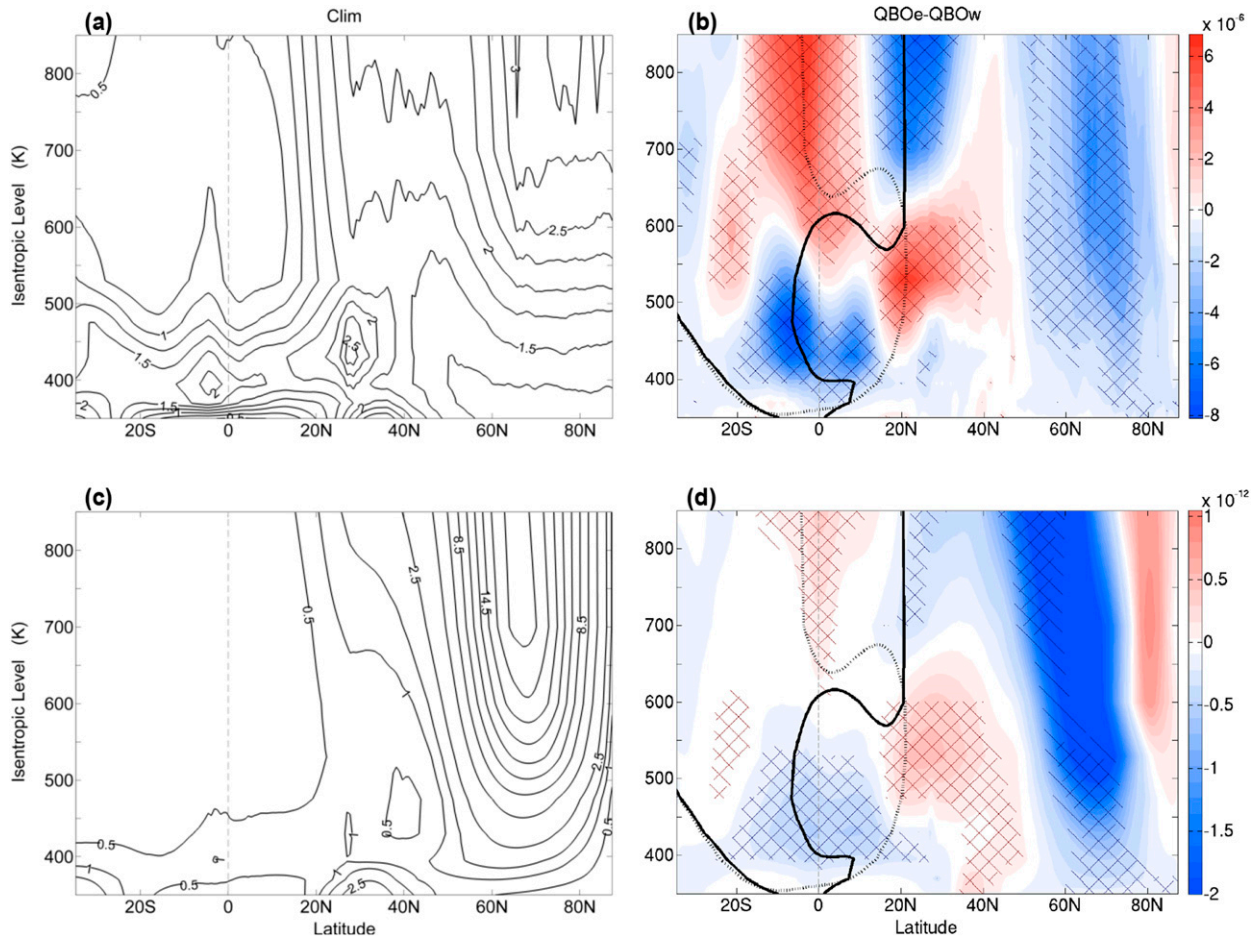


FIG. 5. (a),(b) As in Figs. 2a and 2b, but for $\bar{\xi}$ [units: $\text{K m}^2 \text{kg}^{-1} \text{s}^{-1} (1^\circ)^{-1}$], a wave-activity proxy developed by HH09 (see section 3). The contour interval in (a) is $0.25 \times 10^{-5} \text{K m}^2 \text{kg}^{-1} \text{s}^{-1} (1^\circ)^{-1}$. (c),(d) As in (a) and (b), but for \bar{P}^2 , the wave activity defined in Eq. (5), plotted with contours at $0.5, 1.5, 2.5, \dots \times 10^{-12} \text{K}^2 \text{m}^4 \text{kg}^{-2} \text{s}^{-2}$ and an additional contour at $1 \times 10^{-12} \text{K}^2 \text{m}^4 \text{kg}^{-2} \text{s}^{-2}$ in (c). Note that (c) and (d) have been scaled using a modified PV scaling developed by Lait (1994) in order to visualize the rapid increase of wave amplitude with height; for each isentropic level, we multiply by $(\theta/350)^{-18/2}$.

activity. The DJF climatology and QBO composite difference of $\bar{\xi}$ is shown in Figs. 5a and 5b. As expected, the climatological $\bar{\xi}$ attains its largest values in the NH stratosphere, in particular, poleward of 55°N and with its magnitude increasing with height above 500 K, indicating that the largest variation of PV gradient is associated with the stratospheric polar vortex. Another peak is just above the subtropical jet ($\sim 30^\circ\text{N}$, 400–500 K) suggesting a general convergence of wave activity, which is consistent with the climatological wave breaking near this region (see Fig. 4c). Localized peaks of $\bar{\xi}$ near the tropical tropopause (15°S – 15°N , 360–450 K) are likely to be related to small-scale waves (e.g., Holton 1983).

The $\bar{\xi}$ anomalies in the tropical stratosphere (15°S – 15°N) generally align well with the location of the QBO critical line, with negative $\bar{\xi}$ anomalies in the lower-stratosphere tropics (15°S – 10°N , 400–530 K) and positive $\bar{\xi}$ anomalies in the midstratosphere tropics (15°S – 10°N , 600–850 K). At

15° – 35°N , 475–600 K, the positive $\bar{\xi}$ anomalies could be consistent with wave activity propagating equatorward toward the QBO critical line under QBOe, in agreement with the enhanced \bar{P}_ϕ (Fig. 4b). Negative $\bar{\xi}$ anomalies are found at high latitudes, indicating less wave activity in the region under QBOe, consistent with the negative \bar{u} anomalies (Fig. 2b) and the reduced ability for wave propagation in the region (Figs. 4b,d). However, it is not clear if these high-latitude $\bar{\xi}$ anomalies are a response to, or a cause of, the HTE.

An alternative measure of wave activity, as defined in section 2c, is \bar{P}^2 . The DJF climatology and composite difference of \bar{P}^2 are shown in Figs. 5c and 5d. Seeing as both $\bar{\xi}$ and \bar{P}^2 are heuristic measures of wave activity, the two ought to show qualitatively similar results in terms of their spatial patterns. Indeed, the climatology shows very similar patterns to $\bar{\xi}$, albeit with slight differences in terms of the meridional and vertical extent of

the localized peaks above the subtropical jet and near the tropical tropopause. In the QBO composite difference, $\bar{\xi}$ and $\overline{P'^2}$ anomalies are in broad agreement, with only slight differences in the high-latitude stratosphere and the mid-to-high-latitude upper troposphere–lower stratosphere. At high latitudes, $\overline{P'^2}$ shows significant negative anomalies concentrated along the polar vortex edge, whereas $\bar{\xi}$ shows negative anomalies throughout high latitudes. In the mid-to-high-latitude upper troposphere–lower stratosphere, the latitudinal dipole present in $\bar{\xi}$ at 450–600 K extends down to the 350-K θ level. This indicates enhanced wave activity at midlatitudes under QBOe. Because $\bar{\xi}$ and $\overline{P'^2}$ are similar to each other in both the climatology and composite difference, and also because $\overline{P'^2}$ is featured in the wave-activity conservation law [Eq. (5)], we hereafter refer to $\overline{P'^2}$ as the “wave activity.”

c. Effect on the zonal-mean momentum budget

In this section, the zonal-mean momentum budget [Eq. (2)] is used to determine the effect of the net wave forcing, in terms of the EP flux divergence term Π or the eddy fluxes of PV $\overline{\sigma'v'P'}$, on the stratospheric circulation (see section 2b for equations). We examine the climatology and QBO modulation of the terms in this budget, with a particular focus on providing further explanation of the mechanism governing the HTE.

Figure 6a shows the DJF climatology of the EP flux vectors \mathbf{F} (arrows) and EP flux divergence term Π (contours). The vector \mathbf{F} gives an indication of the direction in which the net wave activity propagates, and Π measures the effect of the waves on the zonal-mean circulation. The zonal-mean wave forcing is marked by upward EP fluxes, which propagate into the stratosphere at midlatitudes and then split into two branches: an equatorward branch in the lower stratosphere at 20°–40°N and an upward branch that is directed along the large values of $\overline{P'_\phi}$ associated with the polar vortex edge (Fig. 4a). At higher θ levels, as the polar vortex becomes stronger (Fig. 2a), more wave activity is guided toward lower latitudes, indicated by the more equatorward-propagating EP fluxes at these higher θ levels. These upward and equatorward EP fluxes are associated with a predominately negative Π and, hence, act to weaken the mean flow [see Eq. (2)]. Positive Π values are noted at 65°–75°N, 775–850 K, which may be an indication of barotropic energy conversion during the latter stages of a baroclinic-wave life cycle (e.g., Simmons and Hoskins 1978) or because of resolved gravity wave forcing.

The QBO composite differences of the DJF-mean \mathbf{F} (arrows) and Π (contours) are shown in Fig. 6b. In the lower stratosphere, the QBO signature is marked by a “fountain like” pattern of the EP flux anomalies at 40°–55°N, whereby upward-propagating EP flux anomalies

spread equatorward toward the QBO critical line and poleward toward the polar vortex, corresponding well with the negative Π anomalies at 20°–40°N and at 60°–80°N, 450–600 K. In the middle stratosphere (700–850 K), poleward EP flux anomalies from the subtropics to high latitudes are accompanied by positive Π anomalies (i.e., divergence) at 20°–40°N and negative Π anomalies (i.e., convergence) at 55°–80°N. The enhanced wave forcing of the mean flow throughout the high-latitude lower to middle stratosphere (450–850 K), as indicated by the negative Π anomalies, is dynamically consistent with the observed HTE.

The relative contributions to the momentum budget of the upward change in form drag $\Pi^{(\theta)}$ and the poleward change in the momentum flux $\Pi^{(\phi)}$, which together add up to the total EP flux divergence term Π , are now examined. Figures 6c and 6e show the DJF climatology of $\Pi^{(\theta)}$ and $\Pi^{(\phi)}$, and Figs. 6d and 6f show their associated QBO composite differences. In terms of the climatology, $\Pi^{(\theta)}$ is predominately negative and becomes increasingly negative in the vicinity of the two strong westerly jets (i.e., the tropospheric subtropical jet and the stratospheric polar vortex). The QBO signature in $\Pi^{(\theta)}$ is characterized by negative anomalies at midlatitudes (35°–55°N) and positive anomalies at high latitudes, with the effect being most significant in the lower stratosphere and becoming weaker in the middle stratosphere. Note that the positive anomalies at high latitudes are only statistically significant over two very small regions. These $\Pi^{(\theta)}$ anomalies suggest that, under QBOe, there is an enhanced convergence of vertically propagating wave activity at midlatitudes that is associated with stronger upward wave forcing outside of the polar vortex in the lower stratosphere.

The climatological $\Pi^{(\phi)}$ tends to have an opposite sign to that of $\Pi^{(\theta)}$, primarily because of the equatorward propagation of the horizontal EP fluxes away from the jets. The predominantly positive $\Pi^{(\phi)}$ values indicate that EP fluxes tend to diverge horizontally away from the jets and toward lower latitudes, where they converge. The QBO signature in $\Pi^{(\phi)}$ divides the NH into three regions, whereby there are negative $\Pi^{(\phi)}$ anomalies in the subtropics and in high latitudes and positive $\Pi^{(\phi)}$ anomalies in midlatitudes. The extratropical $\Pi^{(\phi)}$ anomalies tend to have an opposite sign to that of $\Pi^{(\theta)}$. In the midlatitude lower stratosphere, the anomalous negative $\Pi^{(\theta)}$ and positive $\Pi^{(\phi)}$ cancel one another, resulting in a lack of QBO signal in the total EP flux divergence term Π in this region. Negative $\Pi^{(\phi)}$ anomalies are found in the subtropical lower stratosphere, coinciding with enhanced equatorward wave refraction in this region. At high latitudes, negative $\Pi^{(\phi)}$ anomalies are also found; this is consistent with the reduced equatorward wave refraction (Fig. 6b) and the weaker polar vortex (Fig. 2). The

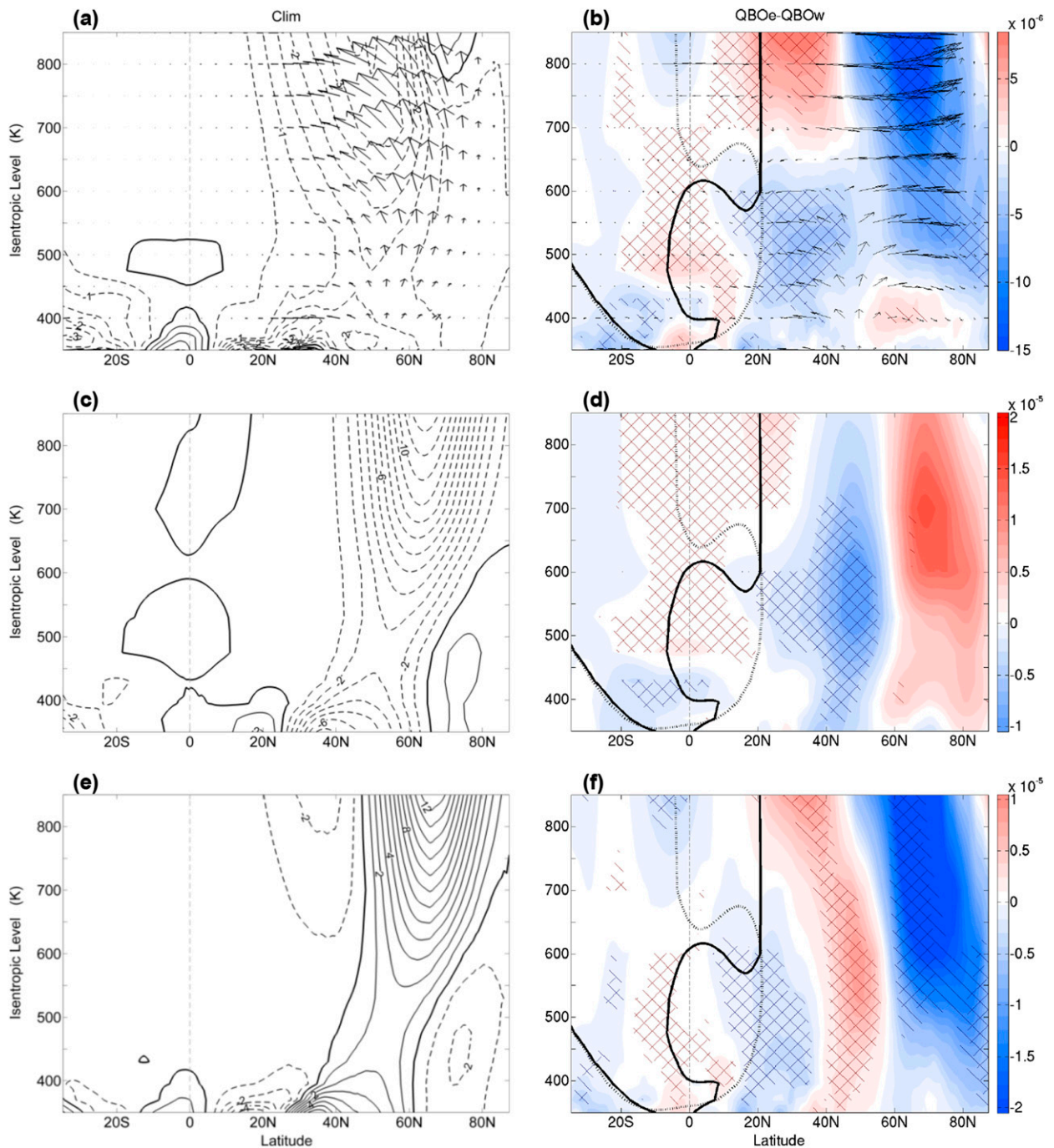


FIG. 6. (a) DJF climatology and (b) DJF composite differences of the EP flux \mathbf{F} and the EP flux divergence term Π . In (a) \mathbf{F} is shown with arrows and Π is shown with the contours (interval: $0.5 \times 10^{-5} \text{ m s}^{-2}$). The EP fluxes have been scaled by σ on each isentropic level to account for the rapid decrease with height of the EP fluxes. Also, the vertical component is multiplied by a factor of 15 000, which was deemed to be suitable to make the magnitudes of $F^{(\varphi)}$ and $F^{(\theta)}$ comparable for better visualization. All the contour lines, the thick solid lines, and dotted lines are as in Fig. 2. (c),(d) As in (a) and (b), but for the vertical component of the EP flux divergence term $\Pi^{(\theta)}$, with a contour interval of $1 \times 10^{-5} \text{ m s}^{-2}$. (e),(f) As in (c) and (d), but for the horizontal component of the EP flux divergence term $\Pi^{(\varphi)}$.

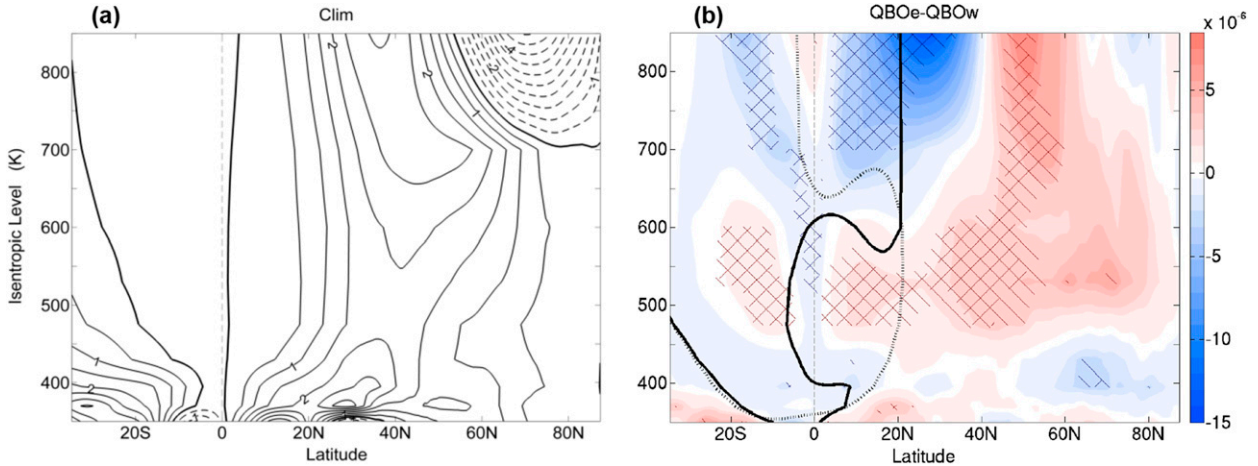


FIG. 7. As in Figs. 2a and 2b, but for the residual mean meridional circulation term Θ . The contour interval in (a) and the value range of (b) are as in Fig. 6a.

high-latitude $\Pi^{(\phi)}$ anomalies have larger magnitude than $\Pi^{(\theta)}$ anomalies and, hence, dominate the total EP flux divergence Π anomalies.

In a seasonal mean, as we analyze here, the net wave forcing Π (Fig. 6) should drive, and hence approximately balance, the residual mean meridional circulation Θ (Fig. 7). In the DJF climatology of Θ , shown in Fig. 7a, this is indeed the case, with a broad balance between the negative Π and the positive Θ , representing an overall northward Brewer–Dobson circulation (BDC). In the high-latitude middle stratosphere (60° – 90° N, 700–850 K), the negative Θ , indicative of an equatorward circulation, coincides with the positive Π . In this region, the magnitude of Θ is evidently larger than that of Π , indicating that other processes, such as gravity wave drag, may play a role.

Figure 7b shows the QBO composite difference of the DJF-mean Θ . The Θ anomalies are broadly in balance and anticorrelated with the Π anomalies, suggesting that the QBO signal in Θ is largely caused by a QBO modulation of the resolved waves. In the lower stratosphere (i.e., 350–600 K), the QBO effect on Θ is marked by an anomalous poleward circulation that extends from the equator to beyond 60° N, indicating an anomalous increase in the strength of the BDC in this region. In the middle stratosphere (i.e., 700–850 K), the QBO effect on Θ is marked by a latitudinal dipole pattern, with anomalous equatorward and poleward circulations at 5° – 35° N and 40° – 65° N, respectively. Overall, the net effect of the QBO modulation of Θ in the lower-to-middle stratosphere is a stronger poleward circulation northward of 40° N, implying an enhanced adiabatic heating in high latitudes and therefore a weaker, more disturbed polar vortex under QBOe. It should be noted that the vertical two-cell structure in the subtropics to midlatitudes is

associated with the QBO-induced meridional circulation (Plumb and Bell 1982). The seasonal asymmetry of this circulation (Kinnersley 1999) is also visible.

An alternative way to determine the net wave forcing of the zonal-mean circulation is to calculate the eddy PV flux term $\overline{\sigma v'P'}$, which is related to the EP flux divergence term Π via Eq. (4). The DJF climatology of $\overline{\sigma v'P'}$ is shown in Fig. 8a. The predominant feature of the climatology is the negative $\overline{\sigma v'P'}$ (indicating equatorward eddy PV fluxes) that peaks along the polar vortex edge. This shows that the effect of the wave drag is to flatten the highly positive PV gradients associated with strong westerly jets by fluxing high PV into lower latitudes, which results in a weaker polar vortex. In the upper troposphere, $\overline{\sigma v'P'}$ is also predominately negative, except for a small region of positive $\overline{\sigma v'P'}$ (i.e., poleward eddy PV fluxes) on the poleward flank of the subtropical jet. It should be noted that the climatological $\overline{\sigma v'P'}$ is broadly in agreement with the EP flux divergence term Π (Fig. 6a) and, hence, approximately balances the meridional circulation term Θ (see Fig. 7a), as expected from Eqs. (2) and (4). The only noticeable difference is in the high-latitude middle stratosphere (poleward of 60° N, 750–850 K), where $\overline{\sigma v'P'}$ is more negative than Π .

The QBO composite difference of $\overline{\sigma v'P'}$ (Fig. 8b) shows a similar structure to the climatology, with the $\overline{\sigma v'P'}$ anomalies broadly agreeing with Π anomalies and roughly balancing those of the meridional circulation term Θ . The anomalous negative $\overline{\sigma v'P'}$ in the subtropical-to-midlatitude lower stratosphere suggest that higher PV values are anomalously fluxed from high latitudes under QBOe, contributing to the enhanced \overline{P}_{ϕ} in this region (see Fig. 4b). Such enhancement of \overline{P}_{ϕ} permits increased wave propagation and, consequently, allows more wave

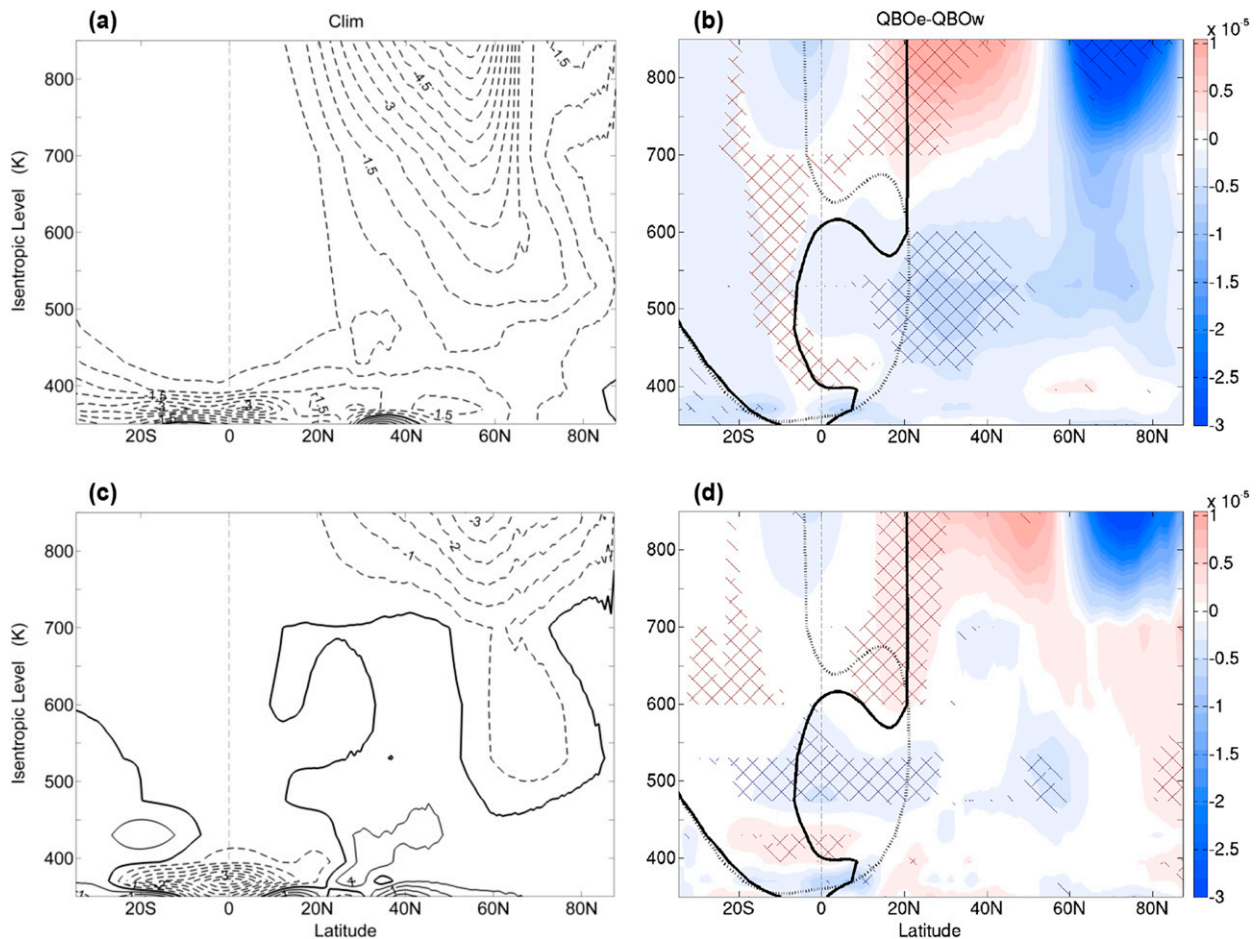


FIG. 8. (a),(b) As in Figs. 2a and 2b, but for $\overline{\sigma'v'P'}$. The contour interval in (a) and the value range in (b) are as in Fig. 7. (c),(d) As in (a) and (b), but for the contribution of other processes, including small-scale gravity waves, nonconservative processes, and nonlinear effects to $\overline{\sigma'v'P'}$. It is calculated from Eq. (4) as $D = \overline{\sigma'v'P'} - \Pi$.

activity to converge in this region (see Figs. 5b, 5d, and 6b). In the middle stratosphere, a dipole pattern exists with positive (i.e., poleward) $\overline{\sigma'v'P'}$ anomalies in the subtropics to midlatitudes (15°–40°N), and negative (i.e., equatorward) $\overline{\sigma'v'P'}$ anomalies at high latitudes (60°–85°N). This dipole pattern indicates a meridional redistribution of PV with poleward displacements of low PV and equatorward displacements of high PV. These displacements of PV would induce low- and high-PV anomalies around a latitude circle near the edge of the polar vortex, indicative of wave growth. This is dynamically agreeable to the HTE.

The difference between the eddy PV flux term $\overline{\sigma'v'P'}$ and the EP flux divergence term Π [see Eq. (4)] allows us to estimate the net contribution $D = -(\overline{\sigma'u'})_t/\overline{\sigma} + D_2 + O(3)$, consisting of small-scale gravity wave effects, nonconservative processes, and higher-order nonlinear terms to the zonal-mean momentum budget. The DJF climatology and composite difference of

D are shown in Figs. 8c and 8d. The climatological D is marked by negative values in the extratropical middle stratosphere, attaining its most negative values in the vicinity of the polar vortex and noticeably weaker values in the lower stratosphere. The net contribution also attains a negative peak near the tropical tropopause and a positive peak value in the midlatitude upper troposphere. The former is known to be affected by gravity waves (Holton 1983; McFarlane 1987), while the latter could be because of the generation of inertia-gravity waves by baroclinic instability (O'Sullivan and Dunkerton 1995) or the nonlinear upscaling from synoptic waves to planetary waves via wave-wave interactions (Birner et al. 2013).

The QBO composite difference of D in Fig. 8d shows negative anomalies in the midlatitude lower stratosphere (45°–60°N, 450–525 K) indicating that small-scale gravity waves, nonconservative effects, and/or nonlinear processes may also play a role in the region where the fountain-like feature appears in the EP flux anomalies

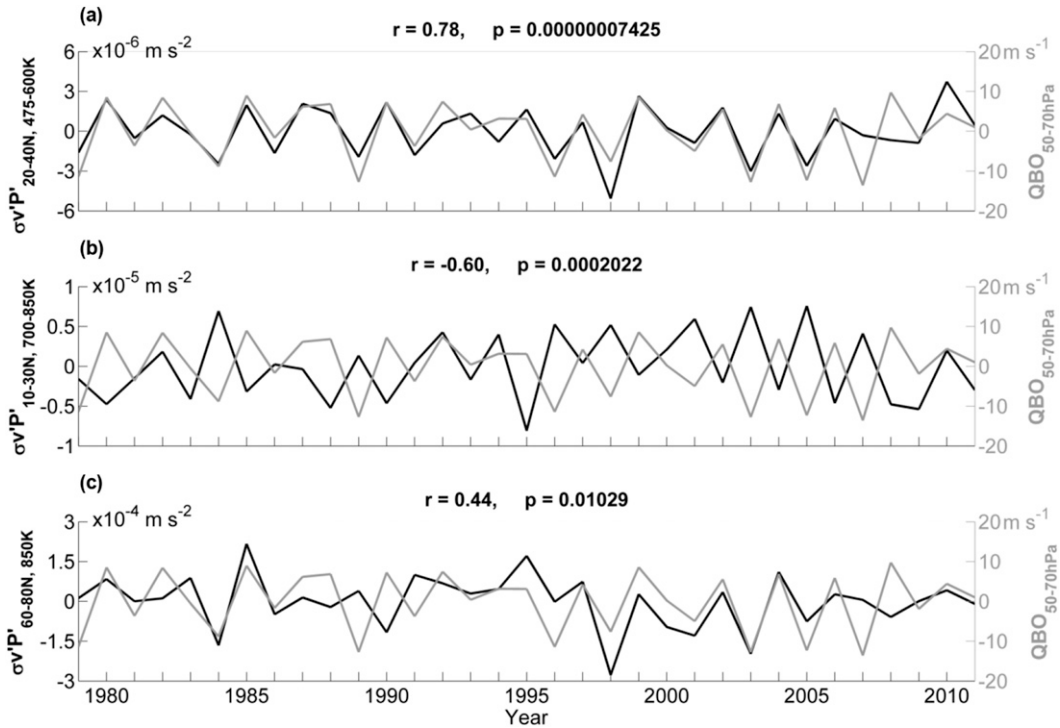


FIG. 9. (a) Time series of DJF mean of $\overline{\sigma v'P'}$ area weighted over 20° – 40° N and 475–600 K (black line), against the seasonal-mean QBO (estimated as the anomalous wind shear between 50 and 70 hPa; gray line). The correlation r and p values are given just above the plot. (b) As in (a), except $\overline{\sigma v'P'}$ is averaged over 10° – 30° N and 700–850 K. (c) As in (a), except $\overline{\sigma v'P'}$ is averaged over 60° – 80° N and 850 K.

(Fig. 6b). Further, the lack of signal in the extratropical middle stratosphere implies that the QBO modulation of wave forcing in this region is mainly due to resolved waves. The vertical dipole structure in the subtropics, with negative D anomalies in the lower stratosphere and positive D anomalies in the middle stratosphere, shares the same sign as those associated with the EP flux divergence term Π ; this possibly implies that the QBO modulation of unresolved subgrid processes, such as small-scale gravity waves in this region, is similar to its effect on resolved waves. This vertical dipole structure in the vicinity of the QBO critical line represents the QBO wave forcing (e.g., gravity wave drag and radiatively damped equatorial waves).

The temporal behavior of the QBO modulation of the DJF-mean $\overline{\sigma v'P'}$ is shown in Fig. 9, where $\overline{\sigma v'P'}$, area averaged over 20° – 40° N and 475–600 K (Fig. 9a), 10° – 30° N and 700–850 K (Fig. 9b), and 60° – 80° N at 850 K (Fig. 9c), is plotted against the QBO. These three regions are selected to represent the most statistically significant NH regions shown in Fig. 8b. The most significant correlation is in the region of 20° – 40° N and 475–600 K, where a correlation coefficient of $r = 0.78$ ($p < 0.01$) is found; this is remarkable given that $\overline{\sigma v'P'}$ is a highly derived quantity. This corroborates the idea that

the QBO plays a dominant role in modulating the wave forcing in this region. In the region of 10° – 30° N at 700–850 K, it is clear that $\overline{\sigma v'P'}$ correlates significantly with the QBO, even though the correlation is visibly contaminated by the volcanic-eruption-affected winters. In the polar middle stratosphere, a correlation coefficient of $r = 0.44$ ($p = 0.01$) is found, consistent with a more-disturbed polar vortex under QBOe.

d. Effect on the wave-activity conservation law

In this section, the wave-activity conservation law [Eq. (5)] is used to identify the regions of wave decay/growth in response to the interactions between waves and the mean flow, given by the up-/downgradient eddy PV fluxes Γ . We analyze the climatology and quantify the first-order (i.e., linear) effect of the QBO on wave decay/growth in the 350–850-K isentropic layer averaged over the winter months of DJF.

Figure 10a shows the DJF climatology of the up-/downgradient eddy PV flux term $\Gamma = 2v'P'\overline{P_\phi}/a$. From Eq. (5), we note that positive Γ , indicative of upgradient eddy PV fluxes, is associated with wave decay ($\partial P'^2/\partial t < 0$), and vice versa. In the climatology, Γ is predominately negative, corresponding to wave growth, and has a magnitude that increases with height and peaks near the edge

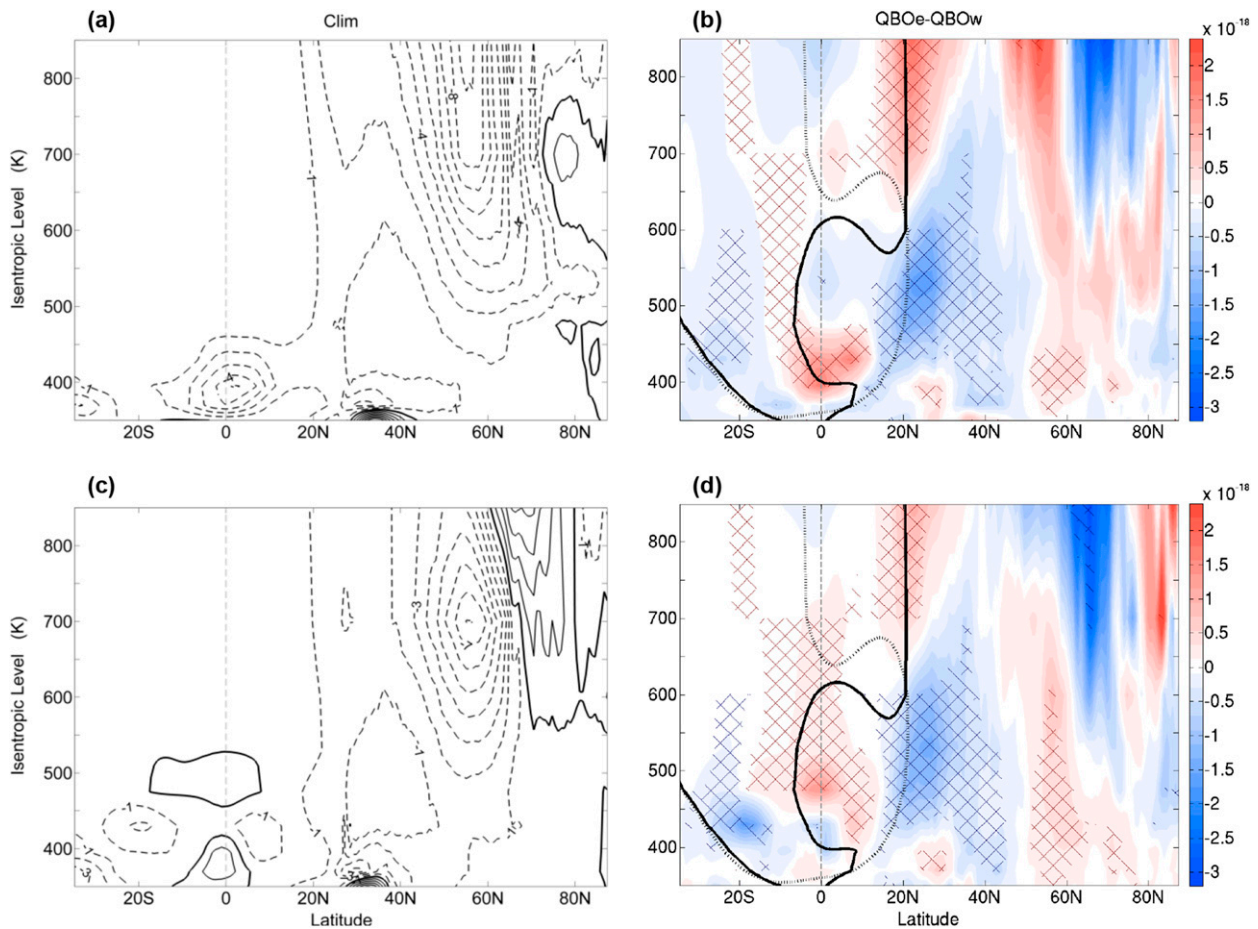


FIG. 10. (a),(b) As in Figs. 2a and 2b, but for the up-/downgradient eddy PV fluxes $\Gamma = 2\overline{v'P'}\overline{P_\phi}/a$ [units: $\text{K}^2\text{m}^4\text{kg}^{-2}\text{s}^{-3}(1^\circ)^{-1}$], where $\Gamma < 0$ corresponds to wave growth ($\partial\overline{P'^2}/\partial t > 0$) and $\Gamma > 0$ corresponds to wave decay ($\partial\overline{P'^2}/\partial t < 0$). The contours in (a) have an interval of $1 \times 10^{-18}\text{K}^2\text{m}^4\text{kg}^{-2}\text{s}^{-3}(1^\circ)^{-1}$. Note that both (a) and (b) have been scaled as in Figs. 5c and 5d. (c),(d) As in (a) and (b), but showing the resolved-wave contribution Γ_{Res} to the wave transience [Eq. (6)], where $\Gamma_{\text{Res}} < 0$ corresponds to wave growth and $\Gamma_{\text{Res}} > 0$ corresponds to wave decay.

of the polar vortex. This supports the diffusive picture of eddy fluxes, whereby eddies tend to flatten the background PV gradient and, hence, weaken the polar vortex (Figs. 2a and 4a; e.g., Rhines and Young 1982). One exception is the small region on the poleward flank of the tropospheric subtropical jet, where positive Γ is found, coinciding with a region of strong positive $\overline{P_\phi}$ (Fig. 4b) and poleward eddy PV fluxes ($\overline{\sigma v'P'} > 0$; Fig. 6b). The wave decay in this region has previously been studied by Birner et al. (2013), who suggested that the poleward shift of the subtropical jet over winter is maintained by an upscaling of synoptic waves. The tropical upper troposphere–lower stratosphere also exhibits negative Γ , corresponding to wave growth, which is mainly because of the contribution of small-scale waves and nonconservative processes to $\overline{v'P'}$ (McFarlane 1987).

The associated QBO composite difference is shown in Fig. 10b. In general, the subtropical anomalies correspond broadly to $\overline{P_\phi}$ anomalies (Fig. 4b), except with

opposite signs. Compared with their SH counterparts, NH Γ anomalies intensify near the QBO critical line, in agreement with enhanced wave breaking near zero-wind lines (Fig. 4d). In the NH lower stratosphere, the subtropical negative Γ anomalies extend into midlatitudes, with accompanying positive Γ anomalies (anomalous wave decay) at $25^\circ\text{--}30^\circ\text{N}$, 350–400 K and $55^\circ\text{--}65^\circ\text{N}$, 350–450 K. Together, they imply that waves favor growth in midlatitudes under QBOe. In the high-latitude middle stratosphere, there appears to be no signal, although the anomalies indicate enhanced wave growth inside the polar vortex and wave decay on its edge, which is in dynamical agreement with the HTE.

The wave decay/growth of the resolved waves is approximated by $\Gamma_{\text{Res}} = 2\overline{P_\phi} \mathbf{V} \cdot \mathbf{F}/a^2\overline{\sigma^2} \cos\phi$ [see Eq. (6)], the DJF climatology of which is shown in Fig. 10c. The Γ_{Res} and Γ climatologies agree broadly from the subtropics to midlatitudes but disagree poleward of 60°N and in the tropical lower stratosphere. More specifically, from

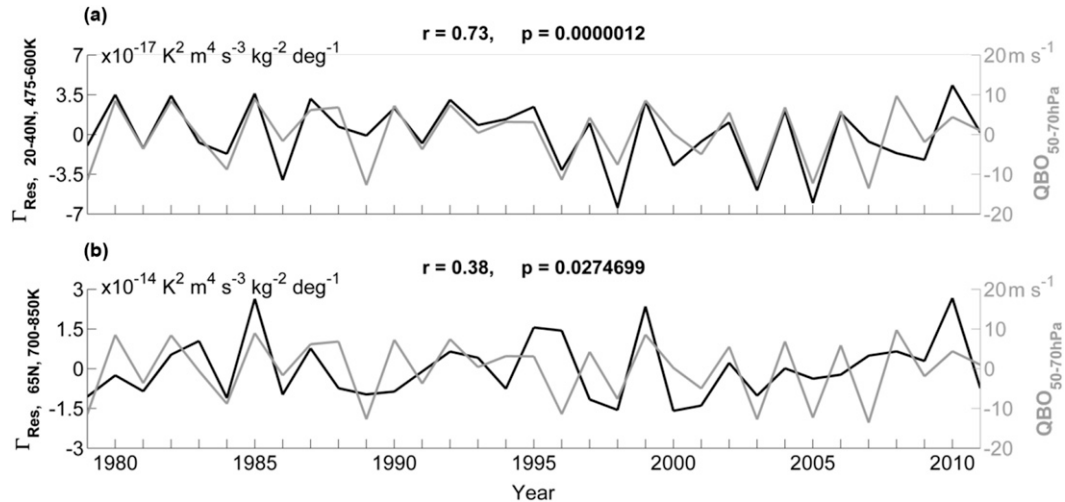


FIG. 11. As in Fig. 3, but showing Γ_{Res} area weighted over (a) 20° – 40° N and 475–600 K and (b) 65° N and 700–850 K.

the subtropics to midlatitudes, both the climatological Γ_{Res} and Γ are predominately negative and peak in the vicinity of the polar vortex edge. Note that almost identical results can be obtained if the perturbation terms in Γ_{Res} are filtered for only the wavenumbers 1–3 (not shown). Thus, the dominant wave forcing in this region is the growth of planetary waves. Conversely, at high latitudes (65° – 80° N, 600–850 K) and in the tropical lower stratosphere, Γ_{Res} has positive values, which is in contrast to the negative Γ in these regions. This implies a downscaling energy conversion process between planetary waves and smaller-scale waves, indicative of an in situ instability. The discrepancies between Γ_{Res} and Γ in these two regions also suggest that other processes, such as small-scale gravity waves and nonconservative effects (as opposed to resolved waves), play an important role.

The QBO composite difference of Γ_{Res} is shown in Fig. 10d; it again highlights a broadly similar pattern to Γ , with exceptions in the tropics and poleward of 55° N. The similarities in the subtropics to midlatitudes support the idea that the QBO effect on wave decay/growth in this region is mainly through a modulation of planetary waves. Nevertheless, two important differences between Γ_{Res} and Γ are found at high latitudes. First, the positive Γ anomalies at 55° – 65° N, 350–450 K are intensified in Γ_{Res} , and the effect extends vertically up to the 550-K θ level, indicating reduced planetary wave growth in the vicinity of the polar vortex in the lower stratosphere. In combination with the increased planetary wave growth at 35° – 50° N, this further indicates enhanced upward wave propagation at midlatitudes under QBOe. Second, the negative Γ_{Res} anomalies at 60° – 65° N, 700–850 K are in dynamical agreement with the poleward increase of horizontal EP flux anomalies in this region (Fig. 6b),

Together, they indicate an in situ planetary wave growth within the polar vortex. These Γ_{Res} anomalies are consistent with a more disturbed polar vortex under QBOe and suggest that planetary waves play a key role in the high-latitude middle stratosphere for the HTE. The lack of signal in Fig. 10b in the high-latitude middle stratosphere in comparison with the Γ_{Res} anomalies at 60° – 65° N, 700–850 K, indicates that other processes may contaminate and, consequently, cancel out the QBO signature in this region.

Figure 11 shows the temporal behavior of the QBO modulation of the DJF-mean Γ_{Res} , which is area averaged over (Fig. 11a) 20° – 40° N, 475–600 K and (Fig. 11b) 65° N, 700–850 K and plotted against the QBO. In the region of 20° – 40° N and 475–600 K, the correlation between the QBO and the resolved-wave decay/growth Γ_{Res} is highly significant ($r = 0.73$, $p < 0.01$). An almost identical result can be obtained if Γ_{Res} is replaced by Γ in this region, confirming that the enhanced wave growth under QBOe in this region is mainly associated with a change of resolved-wave activity. A weaker, yet statistically significant, correlation is found at 65° N, 700–850 K ($r = 0.38$, $p = 0.03$), indicative of there being anomalous planetary wave growth in this region under QBOe, in dynamical agreement with the HTE. However, the correlation coefficient reduces to $r = 0.1$ ($p = 0.74$) when Γ_{Res} is replaced by Γ . This suggests that the anomalous wave growth within the polar vortex under QBOe is predominantly driven by a change of large-scale waves.

5. Conclusions and discussion

For the first time, a systematic examination of the zonal-mean momentum budget and up/downgradient

eddy potential vorticity fluxes, together with three PV-based measures developed by [HH09](#), is utilized to provide a comprehensive description of the climatology and QBO modulation of wave–mean flow interactions in the Northern Hemisphere winter lower-to-middle stratosphere.

Based on the ERA-Interim dataset, we find that the classical Holton–Tan effect (HTE) can be robustly observed during December–February when the relevant variables are mapped to isentropic coordinates. Our analysis of the three PV-based measures provides clear evidence that the QBO modulates wave propagation, wave breaking, and wave activity. At high latitudes, there is enhanced wave breaking, contributing to the weaker polar vortex under QBOe. This is associated with an overall decreased meridional PV gradient and reduced wave activity. In the lower stratosphere, the pattern of PV gradients appears to favor wave activity at midlatitudes and in the vicinity of the QBO-induced critical line.

Our analysis of the QBO modulation of the Eliassen–Palm fluxes and EP flux divergence provide supporting information to the PV-based measures on how the QBO affects wave propagation and the wave forcing of the mean flow. The EP flux anomalies indicate that the enhanced PV gradient in the midlatitude lower stratosphere is associated with increased upward wave propagation. This enhanced upward propagation at 40° – 55° N is accompanied by meridional wave divergence, leading to anomalous horizontal wave convergence both at $\sim 15^{\circ}$ – 45° N, 450–600 K and at high latitudes. In the middle stratosphere, the horizontal EP flux convergence induced by enhanced poleward wave propagation at high latitudes acts to weaken the polar vortex. The overall enhanced stratospheric EP flux convergence drives a stronger poleward meridional circulation, contributing to the warmer high-latitude lower stratosphere under QBOe. Our analysis also suggests that these wave-forcing anomalies are predominantly associated with a change of planetary waves. Overall, these EP flux diagnostics are dynamically agreeable to the HTE.

Analysis of the eddy PV fluxes further supports the general picture that has been obtained from the PV-based measures and the EP flux diagnostics. Under QBOe, enhanced downgradient eddy PV fluxes (indicating wave growth) occur in the lower stratosphere, between the QBO-induced critical line and midlatitudes, in agreement with the equatorward eddy PV fluxes in this region. At 25° – 30° N, 350–400 K and 50° – 65° N, 350–450 K, there are anomalous upgradient eddy PV fluxes (indicating wave decay). This pattern of up-/downgradient eddy PV fluxes in the upper troposphere–lower stratosphere suggests that the enhanced wave growth at midlatitudes is accompanied by wave decay on the equatorward

flank of the subtropical jet and at high latitudes. This pattern seems to form a “valve” for upward wave propagation from the troposphere ([Chen and Robinson 1992](#)), in agreement with the enhanced upward wave propagation at midlatitudes, as shown by the EP fluxes. Downgradient eddy PV fluxes are found in the high-latitude middle stratosphere, indicating planetary wave growth inside the polar vortex; this is in dynamical agreement with the HTE.

Our results show clear and consistent patterns of the QBO modulation of wave activity and wave–mean flow interactions in the extratropics. Nevertheless, they only provide partial support for the classic Holton–Tan (HT) mechanism, whereby a poleward shift in wave propagation and wave activity is expected under QBOe. The QBO signature in the wave-activity measures, however, indicates enhanced wave activity in the midlatitude lower stratosphere and decreased wave activity poleward of 55° N. There is an enhanced upward flux of wave activity into the lower stratosphere at $\sim 40^{\circ}$ – 55° N, which forms a fountain-like feature that diverges horizontally, both equatorward toward the critical line and poleward toward the polar vortex. The poleward EP flux anomalies are associated with an EP flux convergence and increased wave breaking inside the polar vortex, in agreement with the HT mechanism. However, the presence of the equatorward EP flux anomalies in the subtropical-to-midlatitude lower stratosphere and the decrease of wave activity within the polar vortex do not suggest an overall poleward shift of wave forcing under QBOe, as expected by the HT mechanism. Additionally, the enhanced wave growth at midlatitudes with regions of wave decay on the equatorward flank of the subtropical jet and at high latitudes is not explainable by the HT mechanism. These observations are in agreement with recent studies (e.g., [Naoe and Shibata 2010](#); [Yamashita et al. 2011](#); [Garfinkel et al. 2012](#); [Lu et al. 2014](#)) that suggest the HT mechanism is not the dominant mechanism governing the HTE. Nevertheless, caution must be taken with the interpretation of our results, which are based on seasonal averages from December to February. These seasonal averages do not allow us to distinguish the response from the cause and therefore to draw a firm conclusion on the ability of the HT mechanism to explain the observed HTE.

Our comprehensive diagnostics suggest that the change in waveguide associated with the latitudinal shift of the tropospheric subtropical jet may play a role in explaining the HTE. Under QBOe, the QBO-induced meridional circulation appears to cause a poleward shift of the subtropical jet, which consequently encourages upward wave propagation at midlatitudes because of the increased baroclinicity ([Lachmy and Harnik 2014](#)). A

similar shift of the jet was also found by [Garfinkel and Hartmann \(2011\)](#), though the effect they identified is only significant in early and late winter. An enhancement of baroclinicity in the midlatitude lower stratosphere is supported by our zonal-mean momentum budget analysis, whereby there are strengthened zonal-wind anomalies that arch down from the middle stratosphere to the upper troposphere, associated with enhanced wave activity. This is also indicative of a positive feedback, whereby the increased baroclinicity associated with the arching zonal-wind anomalies encourages upward wave propagation from the troposphere, which then diverges meridionally in the fountain-like feature, causing an eddy momentum-flux convergence at midlatitudes and a concurrent strengthening of the zonal-wind anomalies. This, in turn, encourages further upward wave propagation. Accompanying the change in wave forcing in the midlatitude lower stratosphere is a stronger poleward meridional circulation, which aids in the weakening of the polar vortex. Thus, the intensified shift of the subtropical jet under QBOe appears to play a role in the change in wave propagation, and hence wave forcing, and the associated changes in the meridional circulation in the extratropical lower stratosphere.

In light of the aforementioned evidence and drawing on the work of recent studies, we put forward a new, additional mechanism, which has the potential to account for the QBO-induced wave-forcing anomalies in the lower stratosphere during DJF. Under QBOe conditions, this new mechanism works as follows: The QBO-induced mean meridional circulation causes an intensified poleward shift of the subtropical jet in the upper troposphere. The upscaling of wave forcing in the vicinity of the subtropical jet, whereby an excitement of transient planetary waves on the poleward flank of the jet occurs at the expense of synoptic-wave decay ([Birner et al. 2013](#)), is also shifted poleward to midlatitudes. These newly generated planetary waves propagate upward, having a positive feedback with the arching zonal winds in the subtropics to midlatitudes and acting to drive an enhanced poleward meridional circulation in the lower stratosphere, thus contributing to the weaker and warmer polar vortex. The poleward shift of the subtropical jet also results in less baroclinic planetary wave activity at high latitudes, as a result of upward-propagating baroclinic waves favoring propagation toward regions of high baroclinicity (e.g., [Lachmy and Harnik 2014](#)). While our analysis does provide certain evidence for the HTE causality in terms of wave driving, we appreciate that our arguments are based on correlations drawn from reanalysis data. Further work, especially model simulations, must be undertaken to unambiguously determine the validity of this new mechanism.

Previous studies have suggested that the QBO-induced secondary meridional circulation in the middle-to-upper stratosphere may play a role in explaining the HTE (e.g., [Ruzmaikin et al. 2005](#)). Via changes in the background mean-flow geometry, the QBO alters the midlatitude waveguide by affecting the refractive index and causing more poleward wave propagation at 20–5 hPa ([Garfinkel et al. 2012](#); [Lu et al. 2014](#)). Our results in the middle stratosphere are in agreement with those authors, whereby we find that the QBO-induced meridional circulation in the subtropics and the enhanced Brewer–Dobson circulation (BDC) at mid-to-high latitudes correspond to EP flux divergence patterns that are responsible for anomalous poleward wave propagation under QBOe. This reduced equatorward wave refraction above 700 K is dynamically agreeable to the weaker polar vortex. Additionally, this increased poleward wave propagation, in combination with the enhanced planetary wave growth at high latitudes, indicates in situ instability or an energy conversion process from the basic state. If this is the case, the QBO-induced meridional circulation plays very different, albeit complementary, roles in both the lower and middle stratosphere to cause the observed teleconnection between the QBO and the polar vortex via a modulation of planetary wave activity.

The HTE associated with the lower-stratospheric QBO is not necessarily the only layer where a teleconnection between the tropics and the polar vortex occurs. For instance, the QBO-induced subtropical wind anomalies in the upper stratosphere can also contribute to the QBO modulation of wave activity and hence to the HTE (e.g., [Gray et al. 2001, 2004](#)). Such an effect is not studied here because of the height range of the PV dataset we used. Furthermore, our results hint that other processes, such as gravity waves, nonconservative effects, and nonlinear processes may play a role in the vicinity of the QBO critical line, the mid-to-high-latitude lower stratosphere ([Fig. 8d](#)), and the high-latitude middle stratosphere ([Figs. 10b,d](#)). Investigation into such processes may help to improve our understanding of the QBO modulation of wave–mean flow interactions and possible wave–wave interactions in these regions. Finally, an analysis of the seasonal life cycle in terms of the growth and decay of finite-amplitude waves is needed to aid our understanding of the dynamical evolution of the HTE, to better separate the cause and response, and to differentiate the extent to which different mechanisms can play a role. Research regarding the seasonal evolution is currently being undertaken and will be published elsewhere.

Acknowledgments. This study is funded by the Natural Environment Research Council (NERC). We acknowledge the use of the ECMWF reanalysis datasets. We

would also like to thank the two anonymous reviewers whose constructive comments have helped to improve the manuscript. IW is funded by NERC Ph.D. studentship NE/K50094X/1.

REFERENCES

- Abatzoglou, J. T., and G. Magnusdottir, 2007: Wave breaking along the stratospheric polar vortex as seen in ERA-40 data. *Geophys. Res. Lett.*, **34**, L08812, doi:10.1029/2007GL029509.
- Andrews, D. G., 1983: A finite-amplitude Eliassen–Palm theorem in isentropic coordinates. *J. Atmos. Sci.*, **40**, 1877–1883, doi:10.1175/1520-0469(1983)040<1877:AFAEPT>2.0.CO;2.
- , 1987: On the interpretation of the Eliassen–Palm flux divergence. *Quart. J. Roy. Meteor. Soc.*, **113**, 323–338, doi:10.1002/qj.49711347518.
- , J. R. Holton, and C. B. Leovy, 1987: *Middle Atmosphere Dynamics*. International Geophysics Series, Vol. 40, Academic Press, 489 pp.
- Anstey, J. A., and T. G. Shepherd, 2014: High-latitude influence of the quasi-biennial oscillation. *Quart. J. Roy. Meteor. Soc.*, **140**, 1–21, doi:10.1002/qj.2132.
- Baldwin, M. P., and J. R. Holton, 1988: Climatology of the stratospheric polar vortex and planetary wave breaking. *J. Atmos. Sci.*, **45**, 1123–1142, doi:10.1175/1520-0469(1988)045<1123:COTSPV>2.0.CO;2.
- , and T. J. Dunkerton, 2001: Stratospheric harbingers of anomalous weather regimes. *Science*, **294**, 581–584, doi:10.1126/science.1063315.
- , and Coauthors, 2001: The quasi-biennial oscillation. *Rev. Geophys.*, **39**, 179–229, doi:10.1029/1999RG000073.
- Bell, C. J., L. J. Gray, A. J. Charlton-Perez, M. M. Joshi, and A. A. Scaife, 2009: Stratospheric communication of El Niño teleconnections to European winter. *J. Climate*, **22**, 4083–4096, doi:10.1175/2009JCLI2717.1.
- Birner, T., D. W. J. Thompson, and T. G. Shepherd, 2013: Up-gradient eddy fluxes of potential vorticity near the subtropical jet. *Geophys. Res. Lett.*, **40**, 5988–5993, doi:10.1002/2013GL057728.
- Butler, A. H., D. W. J. Thompson, and T. Birner, 2011: Isentropic slopes, downgradient eddy fluxes, and the extratropical atmospheric circulation response to tropical tropospheric heating. *J. Atmos. Sci.*, **68**, 2292–2305, doi:10.1175/JAS-D-10-05025.1.
- Calvo, N., M. A. Giorgetta, R. Garcia-Herrera, and E. Manzini, 2009: Nonlinearity of the combined warm ENSO and QBO effects on the Northern Hemisphere polar vortex in MAECHAM5 simulations. *J. Geophys. Res.*, **114**, D13109, doi:10.1029/2008JD011445.
- Charney, J. G., and P. G. Drazin, 1961: Propagation of planetary-scale disturbances from the lower into the upper atmosphere. *J. Geophys. Res.*, **66**, 83–109, doi:10.1029/JZ066i001p00083.
- Chen, P., and W. A. Robinson, 1992: Propagation of planetary waves between the troposphere and stratosphere. *J. Atmos. Sci.*, **49**, 2533–2545, doi:10.1175/1520-0469(1992)049<2533:POPWBT>2.0.CO;2.
- Dee, D. P., and Coauthors, 2011: The ERA-Interim reanalysis: Configuration and performance of the data assimilation system. *Quart. J. Roy. Meteor. Soc.*, **137**, 553–597, doi:10.1002/qj.828.
- Dunkerton, T. J., and M. P. Baldwin, 1991: Quasi-biennial modulation of planetary-wave fluxes in the Northern Hemisphere winter. *J. Atmos. Sci.*, **48**, 1043–1061, doi:10.1175/1520-0469(1991)048<1043:QBMPW>2.0.CO;2.
- Edouard, S., R. Vautard, and G. Brunet, 1997: On the maintenance of potential vorticity in isentropic coordinates. *Quart. J. Roy. Meteor. Soc.*, **123**, 2069–2094, doi:10.1002/qj.49712354314.
- Garfinkel, C. I., and D. L. Hartmann, 2011: The influence of the quasi-biennial oscillation on the troposphere in winter in a hierarchy of models. Part I: Simplified dry GCMs. *J. Atmos. Sci.*, **68**, 1273–1289, doi:10.1175/2011JAS3665.1.
- , T. A. Shaw, D. L. Hartmann, and D. W. Waugh, 2012: Does the Holton–Tan mechanism explain how the quasi-biennial oscillation modulates the Arctic polar vortex? *J. Atmos. Sci.*, **69**, 1713–1733, doi:10.1175/JAS-D-11-0209.1.
- Gray, L. J., S. J. Phipps, T. J. Dunkerton, M. P. Baldwin, E. F. Drysdale, and M. R. Allen, 2001: A data study of the influence of the equatorial upper stratosphere on northern-hemisphere stratospheric sudden warmings. *Quart. J. Roy. Meteor. Soc.*, **127**, 1985–2003, doi:10.1002/qj.49712757607.
- , S. Sparrow, M. Jukes, A. O'Neill, and D. G. Andrews, 2003: Flow regimes in the winter stratosphere of the northern hemisphere. *Quart. J. Roy. Meteor. Soc.*, **129**, 925–945, doi:10.1256/qj.02.82.
- , S. Crooks, C. Pascoe, S. Sparrow, and M. Palmer, 2004: Solar and QBO influences on the timing of stratospheric sudden warmings. *J. Atmos. Sci.*, **61**, 2777–2796, doi:10.1175/JAS-3297.1.
- Haynes, P. H., and M. E. McIntyre, 1987: On the evolution of vorticity and potential vorticity in the presence of diabatic heating and frictional or other forces. *J. Atmos. Sci.*, **44**, 828–841, doi:10.1175/1520-0469(1987)044<0828:OTEOVA>2.0.CO;2.
- Hitchman, M. H., and A. S. Huesmann, 2007: A seasonal climatology of Rossby wave breaking in the 330–2000-K layer. *J. Atmos. Sci.*, **64**, 1922–1940, doi:10.1175/JAS3927.1.
- , and —, 2009: Seasonal influence of the quasi-biennial oscillation on stratospheric jets and Rossby wave breaking. *J. Atmos. Sci.*, **66**, 935–946, doi:10.1175/2008JAS2631.1.
- Holton, J. R., 1983: The influence of gravity wave breaking on the general circulation of the middle atmosphere. *J. Atmos. Sci.*, **40**, 2497–2507, doi:10.1175/1520-0469(1983)040<2497:TIOGWB>2.0.CO;2.
- , and C. H. Tan, 1980: The influence of the equatorial quasi-biennial oscillation on the global circulation at 50 mb. *J. Atmos. Sci.*, **37**, 2200–2208, doi:10.1175/1520-0469(1980)037<2200:TIOTEQ>2.0.CO;2.
- , and —, 1982: The quasi-biennial oscillation in the Northern Hemisphere lower stratosphere. *J. Meteor. Soc. Japan*, **60**, 140–148.
- , and J. Austin, 1991: The influence of the equatorial QBO on sudden stratospheric warmings. *J. Atmos. Sci.*, **48**, 607–618, doi:10.1175/1520-0469(1991)048<0607:TIOTEQ>2.0.CO;2.
- Hoskins, B. J., M. E. McIntyre, and A. W. Robertson, 1985: On the use and significance of isentropic potential vorticity maps. *Quart. J. Roy. Meteor. Soc.*, **111**, 877–946, doi:10.1002/qj.49711147002.
- Huesmann, A. S., and M. H. Hitchman, 2001: The stratospheric quasi-biennial oscillation in the NCEP reanalyses: Climatological structures. *J. Geophys. Res.*, **106**, 11 859–11 874, doi:10.1029/2001JD900031.
- Jones, D. B. A., H. R. Schneider, and M. B. McElroy, 1998: Effects of the quasi-biennial oscillation on the zonally averaged transport of tracers. *J. Geophys. Res.*, **103**, 11 235–11 249, doi:10.1029/98JD00682.
- Kinnersley, J. S., 1999: Seasonal asymmetry of the low- and middle-latitude QBO circulation anomaly. *J. Atmos. Sci.*, **56**, 1140–1153, doi:10.1175/1520-0469(1999)056<1140:SAOTLA>2.0.CO;2.
- Kunz, T., K. Fraedrich, and F. Lunkeit, 2009: Impact of synoptic-scale wave breaking on the NAO and its connection with the

- stratosphere in ERA-40. *J. Climate*, **22**, 5464–5480, doi:10.1175/2009JCLI2750.1.
- Labitzke, K., 1982: On the interannual variability of the middle stratosphere during the northern winters. *J. Meteor. Soc. Japan*, **60**, 124–139.
- Lachmy, O., and N. Harnik, 2014: The transition to a subtropical jet regime and its maintenance. *J. Atmos. Sci.*, **71**, 1389–1409, doi:10.1175/JAS-D-13-0125.1.
- Lait, L. R., 1994: An alternative form for potential vorticity. *J. Atmos. Sci.*, **51**, 1754–1759, doi:10.1175/1520-0469(1994)051<1754:AAFFPV>2.0.CO;2.
- Lu, H., M. P. Baldwin, L. J. Gray, and M. J. Jarvis, 2008: Decadal-scale changes in the effect of the QBO on the northern stratospheric polar vortex. *J. Geophys. Res.*, **113**, D10114, doi:10.1029/2007JD009647.
- , T. J. Bracegirdle, T. Phillips, A. Bushell, and L. J. Gray, 2014: Mechanisms for the Holton–Tan relationship and its decadal variation. *J. Geophys. Res. Atmos.*, **119**, 2811–2830, doi:10.1002/2013JD021352.
- Marshall, A. G., and A. A. Scaife, 2009: Impact of the QBO on surface winter climate. *J. Geophys. Res.*, **114**, D18110, doi:10.1029/2009JD011737.
- Martius, O., C. Schwarz, and H. C. Davies, 2007: Breaking waves at the tropopause in the wintertime Northern Hemisphere: Climatological analyses of the orientation and the theoretical LC1/2 classification. *J. Atmos. Sci.*, **64**, 2576–2592, doi:10.1175/JAS3977.1.
- Matsuno, T., 1970: Vertical propagation of stationary planetary waves in the winter Northern Hemisphere. *J. Atmos. Sci.*, **27**, 871–883, doi:10.1175/1520-0469(1970)027<0871:VPOSPW>2.0.CO;2.
- McFarlane, N. A., 1987: The effect of orographically excited gravity wave drag on the general circulation of the lower stratosphere and troposphere. *J. Atmos. Sci.*, **44**, 1775–1800, doi:10.1175/1520-0469(1987)044<1775:TEOOEG>2.0.CO;2.
- McIntyre, M. E., 1982: How well do we understand the dynamics of stratospheric warmings? *J. Meteor. Soc. Japan*, **60**, 37–65.
- , and T. N. Palmer, 1983: Breaking planetary waves in the stratosphere. *Nature*, **305**, 593–600, doi:10.1038/305593a0.
- Naito, Y., and I. Hirota, 1997: Interannual variability of the Northern winter stratospheric circulation related to the QBO and the solar cycle. *J. Meteor. Soc. Japan*, **75**, 925–937.
- , and S. Yoden, 2006: Behavior of planetary waves before and after stratospheric sudden warming events in several phases of the equatorial QBO. *J. Atmos. Sci.*, **63**, 1637–1649, doi:10.1175/JAS3702.1.
- Naoe, H., and K. Shibata, 2010: Equatorial quasi-biennial oscillation influence on northern winter extratropical circulation. *J. Geophys. Res.*, **115**, D19102, doi:10.1029/2009JD012952.
- Newman, P. A., E. R. Nash, and J. E. Rosenfield, 2001: What controls the temperature of the Arctic stratosphere during the spring? *J. Geophys. Res.*, **106**, 19 999–20 010, doi:10.1029/2000JD000061.
- O’Sullivan, D., and R. E. Young, 1992: Modeling the quasi-biennial oscillation’s effect on the winter stratospheric circulation. *J. Atmos. Sci.*, **49**, 2437–2448, doi:10.1175/1520-0469(1992)049<2437:MTQBOE>2.0.CO;2.
- , and T. J. Dunkerton, 1995: Generation of inertia–gravity waves in a simulated life cycle of baroclinic instability. *J. Atmos. Sci.*, **52**, 3695–3716, doi:10.1175/1520-0469(1995)052<3695:GOIWIA>2.0.CO;2.
- Pascoe, C. L., L. J. Gray, and A. A. Scaife, 2006: A GCM study of the influence of equatorial winds on the timing of sudden stratospheric warmings. *Geophys. Res. Lett.*, **33**, L06825, doi:10.1029/2005GL024715.
- Plumb, R. A., 2002: Stratospheric transport. *J. Meteor. Soc. Japan*, **80**, 793–801, doi:10.2151/jmsj.80.793.
- , and R. C. Bell, 1982: A model of the quasi-biennial oscillation on an equatorial beta-plane. *Quart. J. Roy. Meteor. Soc.*, **108**, 335–352, doi:10.1002/qj.49710845604.
- Rhines, P. B., and W. R. Young, 1982: Homogenization of potential vorticity in planetary gyres. *J. Fluid Mech.*, **122**, 347–367, doi:10.1017/S0022112082002250.
- Ruzmaikin, A., J. Feynman, X. Jiang, and Y. L. Yung, 2005: Extratropical signature of the quasi-biennial oscillation. *J. Geophys. Res.*, **110**, D11111, doi:10.1029/2004JD005382.
- Simmons, A. J., and B. J. Hoskins, 1978: The life cycles of some nonlinear baroclinic waves. *J. Atmos. Sci.*, **35**, 414–432, doi:10.1175/1520-0469(1978)035<0414:TLCOSN>2.0.CO;2.
- Thompson, D. W. J., M. P. Baldwin, and J. M. Wallace, 2002: Stratospheric connection to Northern Hemisphere wintertime weather: Implications for prediction. *J. Climate*, **15**, 1421–1428, doi:10.1175/1520-0442(2002)015<1421:SCTNHW>2.0.CO;2.
- Tung, K. K., 1979: A theory of stationary long waves. Part III: Quasi-normal modes in a singular waveguide. *Mon. Wea. Rev.*, **107**, 751–774, doi:10.1175/1520-0493(1979)107<0751:ATOSLW>2.0.CO;2.
- Vallis, G. K., 2006: *Atmospheric and Oceanic Fluid Dynamics*. Cambridge University Press, 745 pp.
- Watson, P. A. G., and L. J. Gray, 2014: How does the quasi-biennial oscillation affect the stratospheric polar vortex? *J. Atmos. Sci.*, **71**, 391–409, doi:10.1175/JAS-D-13-096.1.
- Yamashita, Y., H. Akiyoshi, and M. Takahashi, 2011: Dynamical response in the Northern Hemisphere midlatitude and high-latitude winter to the QBO simulated by CCSR/NIES CCM. *J. Geophys. Res.*, **116**, D06118, doi:10.1029/2010JD015016.